

**Letter of Intent to Measure  
the Rare Decay  $K^+ \rightarrow \pi^+ \nu \bar{\nu}$  at the CERN SPS**

**Cambridge, CERN, Dubna, Ferrara, Firenze,  
Mainz, Merced, Perugia, Pisa, Saclay, Sofia,  
Torino**

D. Munday

**Cambridge**

N. Cabibbo, A. Ceccucci\*, V. Falaleev, F. Formenti, B. Hallgren, A. Gonidec,  
P. Jarron, M. Losasso, A. Norton, P. Riedler G. Stefanini

**CERN**

S. Balev, S. Bazylev, P. Frabetti, E. Goudzovski, D. Gurev, V. Kekelidze,  
D. Madigozhin, N. Molokanova, R. Pismenny, Y. Potrebenikov, A Zinchenko

**Dubna**

W. Baldini, A. Cotta Ramusino, P. Dalpiaz, C. Damiani, M. Fiorini,  
A. Gianoli, M. Martini, F. Petrucci, M. Savrié, M. Scarpa, H. Wahl

**Ferrara**

E. Iacopini, M. Lenti, G. Ruggiero

**Firenze**

K. Kleinknecht, B. Renk, R. Wanke

**Mainz**

R. Winston

**Merced**

P. Cenci, M. Piccini

**Perugia**

A. Bigi, R. Casali, G. Collazuol, F. Costantini, L. Di Lella, N. Doble,  
R. Fantechi, S. Giudici, I. Mannelli, A. Michetti,  
G.M. Pierazzini, M. Sozzi

**Pisa**

B. Peyaud, J. Derre

**Saclay**

L. Litov, S. Stoynev, V. Kozhuharov,

**Sofia**

C. Biino, F. Marchetto

**Torino**

# Contents

<b>1</b>	<b>Introduction</b>	<b>4</b>
<b>2</b>	<b>The <math>K \rightarrow \pi\nu\bar{\nu}</math> decays</b>	<b>8</b>
<b>3</b>	<b>The Beam for the <math>K^+ \rightarrow \pi^+\nu\bar{\nu}</math> Experiment</b>	<b>11</b>
3.1	Rationale . . . . .	11
3.1.1	Choice of Accelerator and Primary Proton Momentum . . . . .	11
3.1.2	Comparison with the FNAL Main Injector . . . . .	11
3.1.3	Choice of a Positive Kaon Beam . . . . .	12
3.1.4	Choice of Beam Momentum . . . . .	12
3.2	High-Intensity $K^+$ Beam . . . . .	13
3.2.1	Beam Design and Layout . . . . .	13
3.2.2	Beam Parameters and Estimated Performance . . . . .	17
3.2.3	SPS Availability and Scheduling . . . . .	17
3.3	The Decay Tank . . . . .	20
<b>4</b>	<b>Detectors</b>	<b>21</b>
4.1	CEDAR . . . . .	23
4.2	GIGATRACKER . . . . .	23
4.2.1	The fast pixel detector: SPIBES . . . . .	24
4.2.2	Front-end Electronics and Sensors . . . . .	25
4.2.3	Micromegas-type TPC . . . . .	27
4.3	ANTI . . . . .	28
4.4	Wire Chambers (WC) . . . . .	29
4.5	CHOD . . . . .	30
4.6	LKR . . . . .	32
4.6.1	LKR Control System . . . . .	32
4.7	MAMUD . . . . .	33
<b>5</b>	<b>Trigger</b>	<b>36</b>
<b>6</b>	<b>Electronics, Data Acquisition and DCS</b>	<b>37</b>
<b>7</b>	<b>Suppression of the <math>K^+ \rightarrow \pi^+\pi^0</math> Background</b>	<b>38</b>

---

\*Contact Person, email address: [augusto.ceccucci@cern.ch](mailto:augusto.ceccucci@cern.ch)

<b>8</b>	<b>Preliminary Results from the 2004 Beam Test</b>	<b>42</b>
8.1	Drift Chambers (WC) . . . . .	43
8.2	The NA48/2 KABES Detector . . . . .	43
8.3	Performance of KABES with TDC read-out . . . . .	45
8.4	KABES 25 $\mu\text{m}$ mesh . . . . .	46
8.4.1	Improvement of rate capability . . . . .	46
8.4.2	High rate Behaviour . . . . .	46
8.5	KABES FADC Read-out . . . . .	48
8.5.1	FADC read-out test . . . . .	48
8.5.2	Results from the Test . . . . .	48
8.5.3	Conclusions . . . . .	50
<b>9</b>	<b>Time Schedule</b>	<b>51</b>
<b>10</b>	<b>Resources</b>	<b>52</b>
<b>11</b>	<b>Organization and Conclusions</b>	<b>53</b>

## 1 Introduction

We have investigated the possibility to measure very rare kaon decays at the CERN SPS. The physics motivation is given in Section 2. We have reviewed opportunities to study rare decays of both charged and neutral kaons. In this document we concentrate on charged kaons because the intensity of protons that can be delivered by the current SPS on the T10 target is not a limitation for this programme. We have performed a study for an experiment able to collect about 100  $K^+ \rightarrow \pi^+ \nu \bar{\nu}$  events with a signal to background ratio of 10:1 in two years of data taking. Within the Collaboration we dubbed this initiative NA48/3 for short. The two undetectable neutrinos in the final state require the design of an experiment with redundant measurement of the event kinematics and hermetic vetoes to achieve the necessary background rejection. Particular care has to be taken to suppress the two body decays  $K^+ \rightarrow \pi^+ \pi^0$  and  $K^+ \rightarrow \mu^+ \nu$  which have branching ratios up to  $10^{10}$  times larger than the expected signal. The reconstruction of the two body kinematics may suffer from reconstruction tails and backgrounds can originate if photons from  $K^+ \rightarrow \pi^+ \pi^0$  are not detected or if muons from  $K^+ \rightarrow \mu \nu$  are mis-identified as pions. To suppress backgrounds from the two body decays, kinematics and Particle Identification (PID) have to

be used in conjunction. Backgrounds from  $K^+$  three-body decays need also to be addressed. For convenience we remind the reader of the most frequent  $K^+$  decay modes in Table 1, where they are reported together with the techniques foreseen to reject the backgrounds. The kinematics of the most frequent  $K^+$  decays are compared to that of  $K^+ \rightarrow \pi^+\nu\bar{\nu}$  in

Decay Mode	Branching Ratio	Background Rejection
$K^+ \rightarrow \mu^+\nu$	63%	$\mu$ PID, Two-Body Kinematics
$K^+ \rightarrow \pi^+\pi^0$	21%	Photon Veto, Two-Body Kinematics
$K^+ \rightarrow \pi^+\pi^+\pi^-$	6%	Charged Particle Veto, Kinematics
$K^+ \rightarrow \pi^+\pi^0\pi^0$	2%	Photon Veto, Kinematics
$K^+ \rightarrow \pi^0\mu^+\nu$	3% (called $K_{\mu 3}^+$ )	Photon Veto, $\mu$ PID
$K^+ \rightarrow \pi^0e^+\nu$	5% (called $K_{e 3}^+$ )	Photon veto, $E/p$

Table 1: The most frequent  $K^+$  decay modes.

Figure 1. We plan to use 400 GeV/ $c$  protons from the SPS to perform the experiment. The advantage of using a high energy proton machine such as the SPS is two-fold: the cross section to produce kaons increases as a function of proton energy so that one needs fewer protons to achieve the same kaon flux, thus reducing the non-kaon-related accidental activity. In addition, the higher kaon energy leads to easier photon detection which simplifies the suppression of the backgrounds originating from  $K^+ \rightarrow \pi^+\pi^0$ : for example, employing a 75 GeV/ $c$  kaon beam and limiting the momentum of the reconstructed  $\pi^+$  to 40 GeV/ $c$ , there are at least 35 GeV of electro-magnetic energy from the  $\pi^0$  deposited into the photon vetoes. This reduces significantly the probability that both photons from the  $\pi^0$  decay are left undetected because of photonuclear reactions. The disadvantage of high energy protons and, consequently, high energy secondary beams, is that the pions and the protons cannot be efficiently separated from kaons. The consequence is that the upstream detectors which measure the momentum and the direction of the kaons are exposed to a particle flux about 17 times larger than the useful (kaon) one. It is important to point out that the magnetic spectrometers placed downstream of the decay region do not suffer from the same limitation because:

1. The protons and the undecayed kaons and pions are kept in a vacuum beam-pipe that traverses the spectrometers.
2. The muons from pion decays stay in the beam-pipe without illuminating the drift chambers because of the small transverse momentum released by the pion decay.

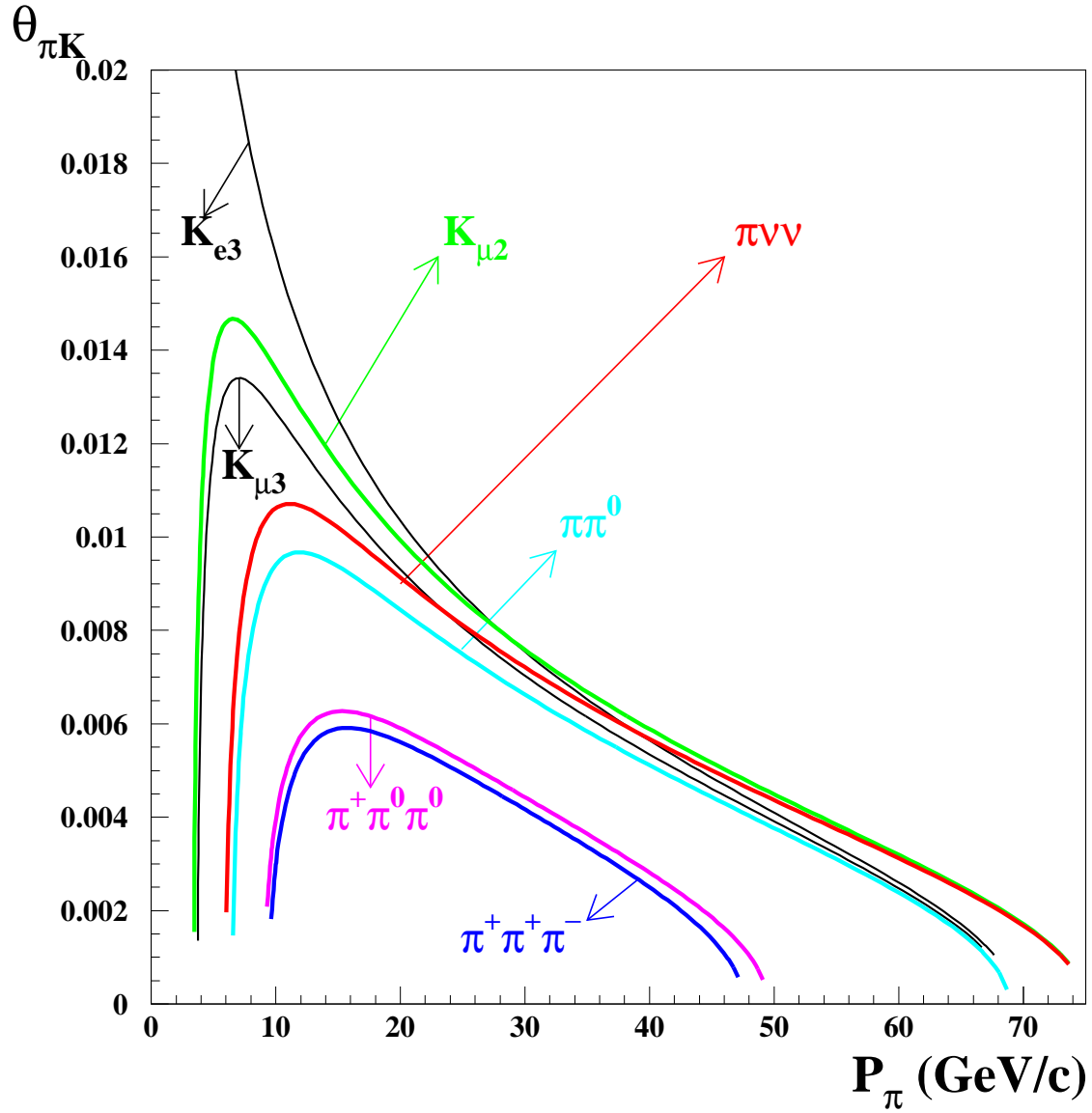


Figure 1: A comparison of the charged track angle-momentum relation for the most frequent  $K^+$  decays and  $K^+ \rightarrow \pi^+ \nu \bar{\nu}$ . For the three body decays, the curves indicate the kinematical limit.

In Section 3 the kaon beam will be described. The experiment is not limited by the flux of protons that can be delivered by the SPS. We assume a duty cycle of the SPS similar to the one available during the 2003 and 2004 data taking.

There are several challenging aspects for this experiment. They include:

- Performing tracking at 1 GHz total rate,  $\sim 40$  MHz/cm<sup>2</sup>, within a minimal material budget, minimal detector dead-time, and excellent time resolution.
- Achieving positive kaon identification in a high rate environment by means of a differential Cherenkov counter insensitive to pions and protons with minimal accidental mis-tagging.
- Constructing and operating hermetic photon vetoes to provide a  $\pi^0$  rejection in excess of  $\sim 10^7$ .
- Achieving a muon rejection of at least  $10^5$ .
- Performing redundant measurement of the momentum of the in-coming  $K^+$  and out-coming  $\pi^+$  for suppression of the tails in the reconstruction of the missing mass for two body decays.
- Vetoing the charged particles coming from kaon decays contained in the area covered by the beam.
- Minimising the accidental activity from non-kaon decays (e.g. muons from the proton dump and tracks coming from pion and kaon decays occurring upstream of the decay region).

We attempt to use as much as possible of the NA48 detectors and infrastructure to keep the cost of the new experiment reasonable. However, significant upgrades are needed. To plan for these upgrades, we have started a detailed simulation of the new experiment and we have collected charged kaon decays at beam rates similar to those planned for NA48/3 during the last week of NA48/2 data taking in 2004. The data taking conditions for these tests and very preliminary results are reported in Section 9. It is important to place this initiative in the world context. So far the study of the decay  $K^+ \rightarrow \pi^+ \nu \bar{\nu}$  has been performed with kaon decays at rest. BNL-AGS-E787 has collected data from 1995 until 1998 and has published [1] a measurement of the branching ratio  $BR(K^+ \rightarrow \pi^+ \nu \bar{\nu}) = 1.57_{-0.82}^{+1.75} \times 10^{-10}$  based on two events interpreted as signal. The follow-up experiment BNL-AGS-E949 [2] has collected data

in 2002 and may collect more data in the future possibly to reach 10 signal events. Plans to pursue further the decay-at-rest technique at the J-PARC have been expressed [3]. As far as decay-in-flight is concerned, the CKM [4] Collaboration has proposed an experiment to measure 100  $K^+ \rightarrow \pi^+ \nu \bar{\nu}$  at the Fermilab Main Injector. The design emphasises the separation of the pions and protons from the kaons in the beam. The experiment was not ratified by the HEPAP P5 sub-panel for cost reasons. The proponents are trying to reduce the cost of the experiment preserving as much physics potential as possible. For such important measurements, to have independent experiments is very important as we learned, for example, from the  $\epsilon'/\epsilon$  experience.

## 2 The $K \rightarrow \pi \nu \bar{\nu}$ decays

The rare decays  $K^+ \rightarrow \pi^+ \nu \bar{\nu}$  and  $K_L \rightarrow \pi^0 \nu \bar{\nu}$  are extremely attractive: they offer unique opportunities for testing the Standard Model and deepening our knowledge of the CKM matrix. For a recent review with extensive references of these decays and of the CKM matrix in general, see [5].

At the quark level the two processes arise from the  $s \rightarrow d \nu \bar{\nu}$  process, which originates from a combination of the “Z” penguin — the first two graphs in Figure 2 — and a double W exchange, the third graph.

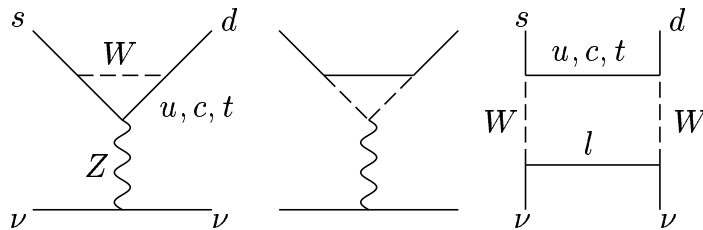


Figure 2: Graphs for  $s \rightarrow d \nu \bar{\nu}$

In these graphs the  $u, c, t$  quarks appear as internal lines, but the top quark contribution dominates, with a smaller contribution, in the case of the  $K^+ \rightarrow \pi^+ \nu \bar{\nu}$  decay, from the charm quark. The up-quark contribution is in both cases negligible, so that  $s \rightarrow d \nu \bar{\nu}$  is essentially a short distance process, well described by a Fermi-like coupling:

$$\mathcal{H}_{eff} = \sum_{l=e,\mu,\tau} \frac{G_l}{\sqrt{2}} (\bar{s}d)_{V-A} (\bar{\nu}_l \nu_l)_{V-A} , \quad (1)$$

where  $G_l$  is the effective coupling constant\*. Given  $G_l$ , the branching ratios are directly related by isospin to that of the  $K_{e3}^+$  decay,

$$B(K^+ \rightarrow \pi^+ \bar{\nu} \nu) = 6r_{K^+} B(K^+ \rightarrow \pi^0 e^+ \nu) \frac{|G_l|^2}{G_F^2 |V_{us}|^2} \quad (2)$$

$$B(K^0 \rightarrow \pi^0 \bar{\nu} \nu) = 6 \frac{\tau_{K_L}}{\tau_{K^+}} r_{K_L} B(K^+ \rightarrow \pi^0 e^+ \nu) \frac{(\text{Im } G_l)^2}{G_F^2 |V_{us}|^2} \quad (3)$$

$r_{K^+} = 0.901$  and  $r_{K_L} = 0.944$  are isospin breaking corrections [6] that include phase space and QED effects. The effective coupling constant  $G_l$  can be expressed as the sum of two contributions, the first arising from an internal top-quark line, the second from a charm quark,

$$G_l = \frac{\alpha G_F}{2\pi \sin^2 \Theta_W} [V_{ts}^* V_{td} X(x_t) + V_{cs}^* V_{cd} X_{NL}^l] \quad (4)$$

where  $x_t = m_t^2/M_W^2$ . The  $X$  coefficients have been computed including the leading QCD corrections [7] [8]. The top quark contribution is precisely known, the main source of error arising from the uncertainty in the value of the  $t$  mass. The smaller contribution from the  $c$ -quark is affected by a larger error.

Averaging over the three neutrino species, the authors of ref. [5] quote the result

$$P_0(X) = \frac{1}{\lambda^4} \left[ \frac{2}{3} X_{NL}^e + \frac{1}{3} X_{NL}^\tau \right] = 0.42 \pm 0.06 . \quad (5)$$

which is reflected in a theoretical error of  $\sim 5 \div 7\%$  on the determination of  $V_{td}$ . This makes the  $K^+ \rightarrow \pi^+ \nu \bar{\nu}$  one of the most attractive tools for the exploration of the unitarity triangle, a member of a very short list of theoretically clean processes.

To evaluate the importance of eqs. (2), (3) and (4), we recall the composition of the CKM matrix in the popular Wolfenstein parameterization [9], whose accuracy is fully sufficient for the present discussion<sup>†</sup>. The parameters  $A$ ,  $\lambda$  can be defined to be positive.

$$V_{\text{CKM}} = \begin{pmatrix} V_{ud} & V_{us} & V_{ub} \\ V_{cd} & V_{cs} & V_{cb} \\ V_{td} & V_{ts} & V_{tb} \end{pmatrix} = \begin{pmatrix} 1 - \frac{\lambda^2}{2} & \lambda & A\lambda^3(\varrho - i\eta) \\ -\lambda & 1 - \frac{\lambda^2}{2} & A\lambda^2 \\ A\lambda^3(1 - \varrho - i\eta) & -A\lambda^2 & 1 \end{pmatrix} + \mathcal{O}(\lambda^4) \quad (6)$$

Comparing with eq. (4), we see that the charm quark contribution to  $G_l$  depends from the well determined elements  $V_{cd}$ ,  $V_{cs}$ , and that this term is (in this approximation) a real

---

\*There is a small difference between the couplings for  $\nu_\tau$  and  $\nu_{e,\mu}$ . Taking for  $G_l$  the average of the three implies a negligible (0.2%) error on the rates.

<sup>†</sup>As discussed [5], the final analysis would use a more exact parametrization and the modified Wolfenstein parameters  $\bar{\rho} = \rho(1 - \lambda^2/2)$  and  $\bar{\eta} = \eta(1 - \lambda^2/2)$ .

number, so that it will not contribute to the  $K_L \rightarrow \pi^0 \nu \bar{\nu}$  decay. The theoretical prediction for this process is thus inherently cleaner than that for  $K^+ \rightarrow \pi^+ \nu \bar{\nu}$ .

Since in our approximation  $V_{ts} = -V_{cb}$ , and the latter is determined accurately from semi-leptonic B decays,  $|V_{cb}| = (41.5 \pm 0.8) \times 10^{-3}$ , a measurement of the branching ratios for the two decays leads to a determination of  $V_{td}$ , i.e of the Wolfenstein parameters  $\rho, \eta$  that define the “unitarity triangle”, which is central to the analysis of the CKM matrix.

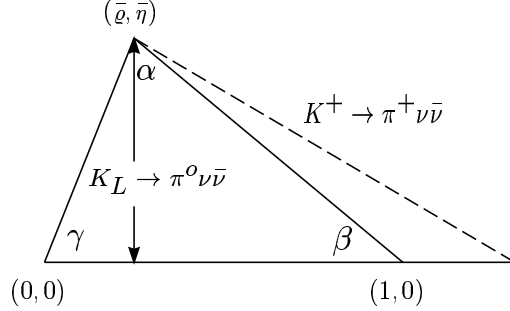


Figure 3: The unitarity triangle; the dashed line represents the measurement of  $K^+ \rightarrow \pi^+ \nu \bar{\nu}$ .

At present the  $\beta$  angle (Figure 3, from [10]) has been determined accurately in B-factory experiments through the  $CP$  violation in  $B \rightarrow \psi K^0$  decays, a process which allows for a very clean theoretical analysis. The length of the right-hand side of the triangle is determined by the analysis of  $B^0 \bar{B}^0$  oscillations, whose theoretical interpretation requires lattice QCD.

The rate of  $K^+ \rightarrow \pi^+ \nu \bar{\nu}$  determines the absolute value of  $G_I$ , which is represented by the dashed segment in Figure 3. The displacement from 1 of the lower extremity of this segment is due to charmed quark contributions. A measurement of this rate would offer a valid alternative to the measurement of  $B^0 \bar{B}^0$  oscillations, but with different, possibly smaller, theoretical uncertainties. Combining the measurement of  $K^+ \rightarrow \pi^+ \nu \bar{\nu}$  with the existing data on  $\beta$  and  $B^0 \bar{B}^0$  oscillations offers [11] a significant test of the Standard Model.

The rate of  $K_L \rightarrow \pi^0 \nu \bar{\nu}$  offers a direct measurement of  $\eta$ , the height of the unitarity triangle. Its detection and measurement would establish the second example of direct  $CP$  violation after the measurement of  $\epsilon'/\epsilon$  in the  $K^0$  system, but with the advantage of a very clean theoretical analysis [12].

The rates of  $K^+ \rightarrow \pi^+ \nu \bar{\nu}$  and  $K_L \rightarrow \pi^0 \nu \bar{\nu}$  offer an accurate determination of the unitarity triangle, which is completely independent from that executed within the B system. As an added enticement,  $K^+ \rightarrow \pi^+ \nu \bar{\nu}$  and  $K_L \rightarrow \pi^0 \nu \bar{\nu}$  are second order weak interaction processes, which probe the short distance behavior of the Standard Model, and could be

sensitive to new physics. An analysis of possible post-Standard Model scenarios is given in [11].

## 3 The Beam for the $K^+ \rightarrow \pi^+ \nu \bar{\nu}$ Experiment

### 3.1 Rationale

#### 3.1.1 Choice of Accelerator and Primary Proton Momentum

Once it is realised that it becomes unrealistic to separate kaons with respect to other charged particles by (super-conducting) r.f. cavities at momenta larger than  $30 \text{ GeV}/c^\ddagger$ , there appear to be distinct advantages in performing a charged kaon, rare decay experiment at high energy and, in particular, at the **400 GeV/c SPS** <sup>§</sup>.

Based on a simple empirical formula, fitting the measured particle production data [13], we derive that, per primary proton of momentum  $p_0$  and for fixed  $K^+$  ( $K^-$ ) momentum,  $p_K$ :

- the maximum  $K^+$  ( $K^-$ ) production in a given momentum bite  $\Delta p/p$  and solid angle occurs for  $p_0 \approx 8.5 p_K$  ( $\approx 13 p_K$ ),
- whereas, for fixed  $p_0$ , the maximum  $K^+$  ( $K^-$ ) production occurs at  $p_K \approx 0.35 p_0$  ( $\approx 0.23 p_0$ ).

Moreover, at fixed  $p_K/p_0$ :  $K^+$  ( $K^-$ ) production increases as  $p_K^2$  (and therefore as  $p_0^2$ ). Hence: the number of  $K^+$  ( $K^-$ ) decays in a fixed fiducial length is maximum for  $p_K \approx 0.23 p_0$  ( $\approx 0.15 p_0$ ) and, at fixed  $p_K/p_0$ : the number of  $K^+$  ( $K^-$ ) decays in a fixed length increases as  $p_K$  (and therefore as  $p_0$ ). Furthermore, the acceptance, efficiency and resolution of certain detector elements, e.g. photon veto counters, calorimeters and muon detectors, improve at higher energy.

#### 3.1.2 Comparison with the FNAL Main Injector

We may compare the advantages and disadvantages of the CERN-SPS with respect to the only other high energy proton machine: the FNAL Main Injector (MI). Since, in an unseparated beam, the experiment is not proton limited and the MI has a similar duty cycle to the one

---

<sup>‡</sup>The distance between the cavities has to increase as  $p_K^2$ , whereas the kaon decay length increases only as  $p_K$ . Thus the proposed [4] 216 m long, 22 GeV/c, FNAL  $K^+$  beam would suffer from a survival factor of only 0.27 without considering losses from the separation mechanism.

<sup>§</sup>400 GeV/c is the highest proton momentum of the SPS, at which a duty cycle of 0.3 can be sustained.

of the SPS, there is no advantage to perform the experiment at the MI. On the contrary, the fraction of kaons in the SPS is 6 % to be compared to 4 % at the MI. Therefore, for the same fraction of kaons decaying in the fiducial volume, which depends only on the geometry of the experiment, the accidental rate due to unwanted particles per kaon is 50% smaller at the SPS, which is a considerable advantage.

### 3.1.3 Choice of a Positive Kaon Beam

The choice of a positive rather than a negative (unseparated) beam is motivated by the fact that, at a possible beam momentum of 75 GeV/ $c$  (see 3.1.4), the ratio of production rates:  $K^+/K^-$  per 400 GeV/ $c$  proton is  $\approx 2.1$  and the ratio:  $(K^+/\pi^+)/(K^-/\pi^-) \approx 1.2$ , whilst the ratio:  $\frac{(K^+/\text{Total positive beam flux})}{(K^-/\text{Total negative beam flux})} \approx 1.0$ .

### 3.1.4 Choice of Beam Momentum

The tentative choice of 75 GeV/ $c$  as the central beam momentum is a compromise among the criteria for which the variations with momentum (from 400 GeV/ $c$ ) protons at zero production angle<sup>¶</sup>) are listed in Table 2. The  $K^+$  beam fluxes reported in the Table are estimated using an empirical formula, fitting the measured particle production data [13]. The numbers in italics are taken from measurements made at 60 and 120 GeV/ $c$  from 400 GeV/ $c$  protons on 300 and 500 mm Be targets - interpolated to a 400 mm long target. Hence, secondary interactions in the target may contribute to the beam flux, particularly at 60 GeV/ $c$ .

Moreover, 75 GeV/ $c$  appears to be about the maximum momentum for which a beam incorporating stages for large solid angle acceptance, momentum selection,  $K^+$  tagging, beam momentum measurement and tracking, can be constructed using standard (radiation-resistant) beam elements and fitting into the present length of 102 m from production target (T10) to the beginning of the NA48 decay fiducial region.

---

<sup>¶</sup>For the present, we assume a production angle centred around zero, though it may be worth considering another production angle: e.g. at 75 GeV/ $c$ , a 5 mrad central production angle could lead to a factor 1.2 increase in  $K^+ / \text{Total beam flux}$ , however, requiring a factor 1.5 increase in primary proton flux to restore the  $K^+$  yield.

		$p_K$ (GeV/ $c$ )			
		60	75	90	120
$K^+$ beam flux at production	$\times 10^8$	1.1	1.5	1.9	2.4
for $3 \times 10^{12}$ incident protons		<i>1.3</i>			<i>2.3</i>
$K^+$ survival factor over 102 m		0.80	0.83	0.86	0.89
$K^+$ / Total beam flux	$\times 10^{-2}$	5.2	5.5	5.6	5.2
		<i>6.8</i>			<i>4.7</i>
$K^+/\pi^+$ flux	$\times 10^{-2}$	8.3	8.6	9.0	9.7
		<i>11.2</i>			<i>8.6</i>
$K^+$ decays in 50 m	$\times 10^6$	8.9	10.7	11.6	11.4
$K^+$ decays in 50 m / Total beam flux	$\times 10^{-3}$	4.3	3.9	3.4	2.5
$K^+ \rightarrow \pi^+\nu\bar{\nu}$ Acceptance		0.08	0.11	0.12	0.11
(Region I, no $\pi^+$ momentum cut)					
Accepted $K^+ \rightarrow \pi^+\nu\bar{\nu}$ / Total flux	$\times 10^{-13}$	0.34	0.43	0.41	0.21

Table 2: Variation of relevant  $K^+$  production and decay parameters with secondary beam momentum for 400 GeV/ $c$  primary protons. as a function of secondary beam momentum.

## 3.2 High-Intensity $K^+$ Beam

### 3.2.1 Beam Design and Layout

We attempt to design an unseparated beam of positive hadrons, to be derived from an attainable flux of 400 GeV/ $c$  protons, in the SPS North Area High Intensity Facility [14], comprising the underground target and beam tunnel, TCC8, followed by the experimental cavern, ECN3, where the NA48 detectors are now installed. Furthermore, as a first option, we would reuse the existing target station T10 and the present (straight) K12 beam line, of length 102 m to the exit of the final collimator, marking the beginning of the decay fiducial region and leading to the NA48 detectors (notably the liquid krypton e.m. calorimeter, LKR).

Compared to the present, simultaneous  $K^+$  and  $K^-$  beams [15], the single-charge beam would start with a triplet of radiation-resistant quadrupole magnets to collect a large solid angle acceptance at 75 GeV/ $c$  central momentum, and to provide a focus in the vertical plane at the longitudinal position of the proton beam-dump (TAX). This is located (as in the present beam) at the centre of a 'front-end achromat', consisting of four, radiation-hard

dipole magnets, the first pair of which displace the 75 GeV/c beam vertically by 100 mm onto a momentum-defining slit contained in the TAX to permit the selection of a narrow ( $\simeq 1\% \Delta p/p$ ) momentum band. The second pair of magnets then return the wanted particles onto the undeviated axis. Thereafter, a pair of quadrupoles focuses the beam through redefining collimators in both planes. In between these, it passes through a 60 mm diameter, field-free bore traversing magnetic iron blocks, filling the normal gap of a pair of large dipole magnets, which serve to sweep aside muons accompanying the beam. A further pair of quadrupoles renders the beam parallel at the location of an upgraded, helium gas-filled, CEDAR differential Cerenkov counter [16], capable of tagging only the  $K^+$  in the beam. A final pair of quadrupoles produces a beam which converges slightly towards a waist, located close to the detectors of the experiment. The last 30 m length to the final collimator incorporates a 'second achromat' of four dipole magnets and three sets of tracking detectors to provide momentum and direction measurements on all particles. Upstream of the final collimator the beam is surrounded by a pair of 5 m-long, magnetic iron 'scrapers' of 60 mm horizontal and vertical aperture, respectively. They are toroidally magnetised so as to defocus  $\mu^+$  around the beam. The layout and optics of the beam, calculated using TRANSPORT [17], are shown schematically in Figure 4.

The decay fiducial region is housed in a large,  $\approx 100$  m long vacuum tank, which is closed off by a thin ( $3 \times 10^{-3} X_0$ ) Kevlar-composite membrane (or 'window'). At its centre it is traversed by a thin-walled aluminium beam tube of  $\approx 160$  mm inside diameter, which allows the beam to be transported in vacuum through all the principal detectors of the experiment. This part of the layout is shown schematically in Figure 5.

The detector components are described in later Sections. Of relevance for the beam are a double magnetic spectrometer, comprising tracking chambers (WC 1 - 6) covering the full acceptance outside the central beam tube, interspaced by two (similar), large-aperture dipole magnets (MNP33-1 and MNP33-2). These are chosen to provide horizontal  $p_T$ -kicks of  $-157.5$  MeV/c and  $+262.5$  MeV/c, thereby deflecting the 75 GeV/c beam by  $-2.1$  and  $+3.5$  mrad, respectively. Beam and associated particles (e.g. muons) of all momenta are thus centred on the axis again downstream of the LKr calorimeter, where a combined magnetised-iron hadron calorimeter and muon detector (MAMUD) is located. This is designed to produce a  $\approx +1350$  MeV/c horizontal  $p_T$ -kick on the beam, causing a further  $+18$  mrad deflection. The beam is hence displaced 160 mm off axis 8 m further downstream (at the extremity of ECN3), so as to clear a 100 mm radius detector (SAC3). Together with an annular detector around the centre of the Kevlar window (SAC1), possibly others around the beam

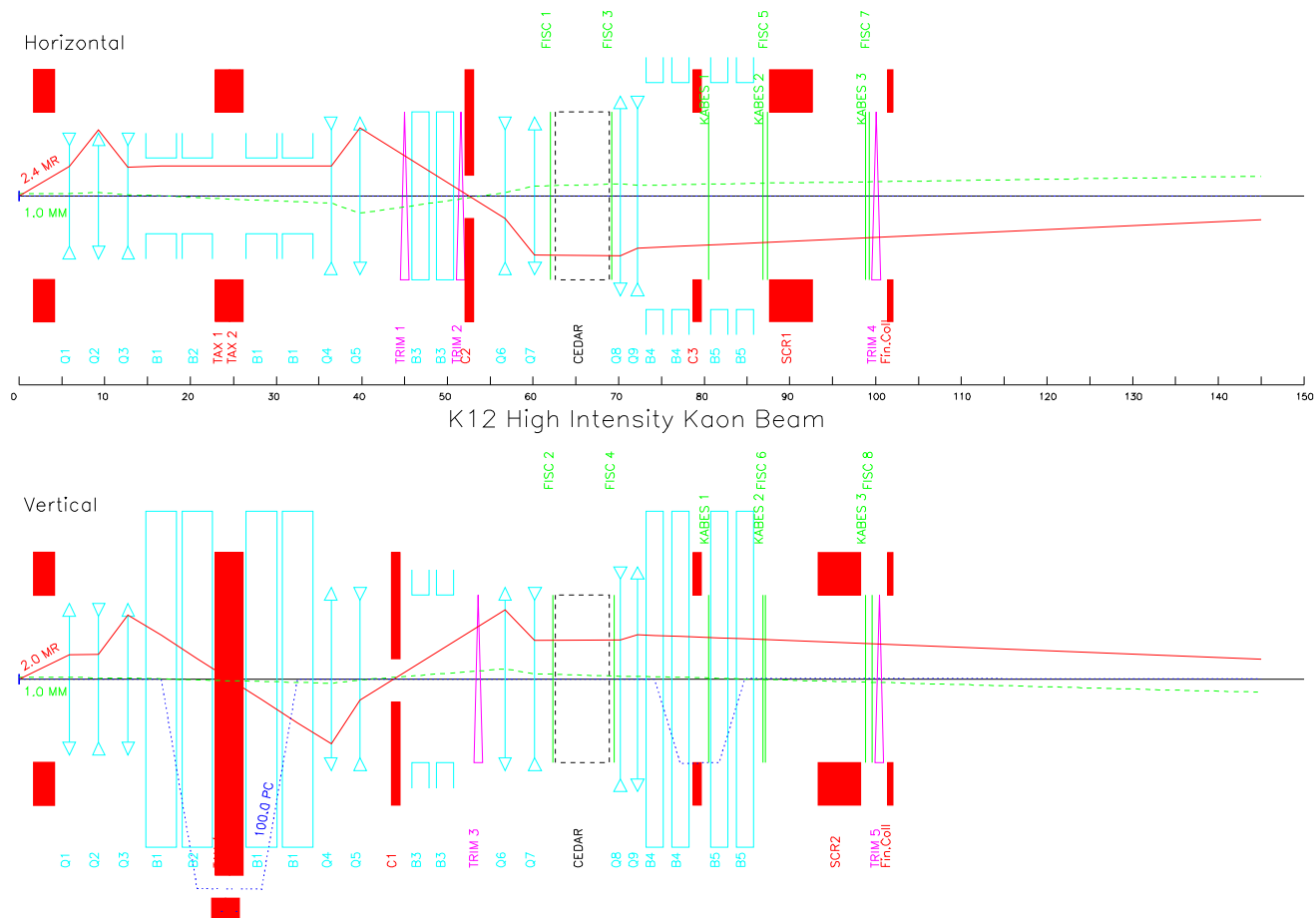


Figure 4: Schematic layout and optics of the high intensity  $K^+$  beam

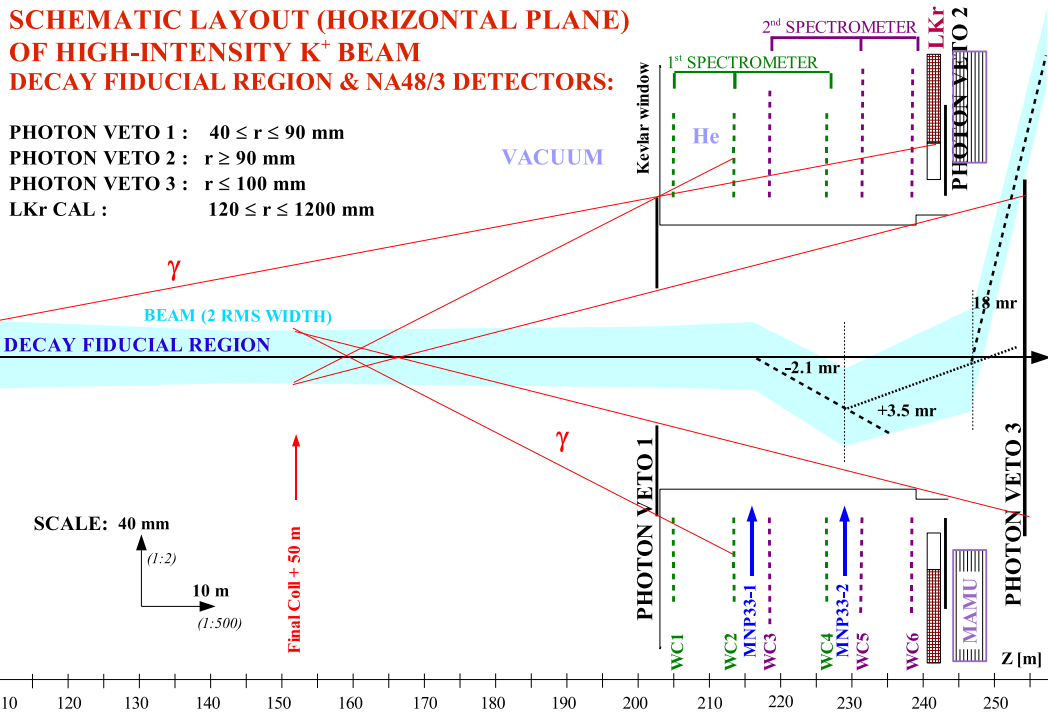


Figure 5: Schematic layout of beam and detectors incorporating Small Angle PHoton Vetoes (SAC).

tube (SAC2), and in addition to the LKR calorimeter itself, this system of photon detectors is designed to provide hermetic veto coverage for photons originating in the decay fiducial region.

### 3.2.2 Beam Parameters and Estimated Performance

The principal parameters of the possible high-intensity  $K^+$  beam are listed in Table 3, where the factors responsible for the flux yield are compared with those for the present K12 simultaneous  $K^+$  and  $K^-$  beam, designed for experiment NA48/2 [15]. The effective solid angle and momentum acceptance, as well as the beam sizes and divergences of both beams were calculated using the ray-tracing programme TURTLE [18]. The particle fluxes of the present beam are taken from the actual measurements made at 60 GeV/ $c$  [13], whereas those for the proposed 75 GeV/ $c$  beam are derived from the latter by extrapolation using the empirical formula proposed in [13].

The muons accompanying a high-energy, high-intensity, secondary beam contribute a major part of the single particle flux, to which the detectors outside the beam are exposed. The transport and decay to  $\mu^\pm\nu$  of a wide spectrum of  $\pi^\pm$  and  $K^\pm$  originating in the target has been simulated and the layout of muon-deflecting elements optimised using the programme HALO [19]. This tracks the parent particles and their decay muons inside the beam apertures and the 'halo' muons leaving the apertures through the vacuum tubes, magnet yokes and shielding surrounding the beam. The preliminary results of such calculations are summarised in Table 4. It appears that the flux of halo muons traversing the main detectors (e.g. WC1 — WC6) can be reduced to  $\approx 2 \times 10^7$  per pulse of  $3 \times 10^{12}$  protons on target (i.e.  $\approx 7MHz$ ).

### 3.2.3 SPS Availability and Scheduling

The conclusion can be drawn from Table 3 that, with an effective overall data-taking efficiency (SPS and detector) of 0.67 and a useful  $K^+ \rightarrow \pi^+\nu\bar{\nu}$  acceptance of 0.1, about 40 events would be accumulated in a year of  $\approx 4.5 \times 10^5$  scheduled fixed-target proton spills (of 4.8 s duration at 400 GeV/ $c$ ) for a Branching Ratio  $BR(K^+ \rightarrow \pi^+\nu\bar{\nu}) = 10^{-10}$ .

This exceeds by a factor  $\approx 1.5$  the number of proton spills per year scheduled for NA48/1 and NA48/2 in recent years AND by factors of  $\approx 2.5$  ( $\approx 1.5$ ) the typical number of spills predicted to be available for fixed target physics, according to various upgrade options in the years 2007 (2010), taking into account the needs of CNGS and LHC [20].

This Letter of Intent is therefore based on the assumption that, by the time such an experiment could be ready to take data, there would be no heavy ion programme, nor any

Beam	Present K12 (NA48/2)	New High Intensity $K^+$ (NA48/3)	Factor w.r.t. present
SPS protons per pulse	$1 \times 10^{12}$	$3 \times 10^{12}$	3.0
Duty cycle (s / s)	4.8 / 16.8	same	1.0
Beam Acceptance H,V (mrad)	$\pm 0.36$	$\pm 2.4, \pm 2.0$	
Solid Angle ( $\mu$ sterad)	$\simeq 0.40$	$\simeq 16$	40
Central $K^+$ Momentum < $p_K$ > (GeV/c)	60	75	$K^+$ : 1.50 $\pi^+$ : 1.35 Total: 1.35
Momentum band $\Delta p_K$ GeV/c	63-57 = 6	76.1-73.9=2.25	$\simeq 0.375$
Eff.: $\Delta p/p$ (%)	$\pm 5$	$\pm 1.5$	$\simeq 0.3$
RMS: $\Delta p/p$ (%)	$\simeq 4$	$\simeq 0.95$	$\simeq 0.25$
Beam size (cm)	$\pm 1.5$	$\pm 2.5$	
Area at GIGATRACKER (cm <sup>2</sup> )	$\simeq 7$	$\simeq 20$	$\simeq 2.8$
Divergence: RMS (mrad)	$\simeq 0.05$	$\simeq 0.1$	$\simeq 2$
Decay fid. length (m)	50	50	
( $\tau_{K^+}$ )	0.11	0.09	0.8
Beam flux/pulse( $\times 10^7$ ): protons	0.86	49	
$K^+$	0.31	15	50 ( $\simeq 30$ )
$\pi^+$	3.32	150	45 ( $\simeq 27$ )
$e^+$	0.95	35	
Total beam flux per pulse ( $\times 10^7$ )	5.5	250	$\simeq 45$ ( $\simeq 27$ )
Rate (3s eff. spill length) (MHz)	18	800	$\simeq 45$ ( $\simeq 27$ )
Rate in GIGATRACKER (MHz/cm <sup>2</sup> )	2.5	40	$\simeq 16$ ( $\simeq 10$ )
Effeciency $\times$ Running time/yr (days)	$1/2 \times 120$	$2/3 \times 90$	
(pulses)	$1/2 \times 6 \times 10^5$	$2/3 \times 4.5 \times 10^5$	1.0
$K^+$ decays per year	$1.0 \times 10^{11}$	$4 \times 10^{12}$	$\simeq 40$
$K^+ \rightarrow \pi^+ \nu \bar{\nu}$ Events/year (BR= $10^{-10}$ , accept. = 10%)		40	

Table 3: A comparison between the current NA48/2 beam and the future one. The figures in brackets in the last column refer to increase in rate with respect to the sum of the positive and negative NA48/2 beams.

<b>FLUX</b> $\times 10^6$ for $10^{12}$ interacting p in H $\approx 3 \times 10^{12}$ incident p on Be	$\pi^+ \rightarrow \mu^+\nu$	$K^+ \rightarrow \mu^+\nu$	$\pi^- \rightarrow \mu^-\bar{\nu}$	$K^- \rightarrow \mu^-\bar{\nu}$	TOTAL
$\pi$ and $K$ at exit final coll. (T10 + 102.0 m)	1956.0	136.5	0	0	2092.5
$\mu$ in beam at final coll.	<i>1500</i>	<i>150</i>			<i>1650</i>
$\mu$ 'HALO' exit final coll.	25.75	1.75	0	0	27.5
	3.25	1.5	2.5	0	7.25
$\pi$ and $K$ at WC 1 (204.9 m)	1912.75	116.25	0	0	2029.0
$\mu$ 'HALO' in WC 1: [2.4 $\times$ 2.4]m <sup>2</sup> , $r > 12$ cm	4.75	12.75	2.5	0.5	20.5
WC 2 (213.7 m)	5.25	12.75	2.5	0.5	21.0
WC 3 (219.1 m)	5.0	12.75	2.5	0.25	20.5
WC 4 (226.3 m)	5.5	13.25	2.5	0.25	21.5
WC 5 (231.7 m)	6.0	13.5	2.5	0	22.0
WC 6 (238.9 m)	5.5	13.5	2.5	0	21.5
	<i>4.2</i>	<i>14.8</i>			<i>21.5</i>
$\pi$ and $K$ deflected to side of SAC3 (254.7 m)	1873.25	104.25	0	0	1977.5
$\mu$ in SAC3: [18 $\times$ 18]cm <sup>2</sup>	1.0	1.25	0	0	2.25

Table 4: Estimated muon halo in the high-intensity  $K^+$  beam. The numbers in italics indicate the  $\pi^+$ ,  $K^+$  fluxes given in Table 3 and the corresponding  $\mu^+$  fluxes renormalised to these.

other experiment in ECN3 competing for proton beam time and that some readjustment of priorities with respect to CNGS could be envisaged. We note that the target number of SPS fixed target spills requested by COMPASS is  $7.2 \times 10^5$  per year [20]. The beam and experiment presented here, requiring  $3 \times 10^{12}$  protons per pulse on target T10 ( $6 \times 10^{12}$  ppp on target T4) is entirely compatible with simultaneous running of COMPASS in the M2 beam ( $\approx 1.2 \times 10^{13}$  ppp on T6) and with experiments or tests in the remaining beams H2, H4, H6 and H8.

In the years 2006 - 2007, before the new beam would be available, we request the use of the existing K12 beam. It can provide a (relatively broad-band) beam of positive hadrons (without particle-identification) around 75 GeV/ $c$ , with a flux up to 16 times that used for experiment NA48/2 [15] (Table 3). Alternatively, it may be used to provide test beams of electrons or muons. The purpose of this programme would be to continue tests, started in 2004, on certain detector elements, to validate their choice for the proposed experiment. In a second phase, possibly starting 2008, we would hope to exploit the new beam to test and calibrate the new detectors as soon as they could be installed.

### 3.3 The Decay Tank

A preliminary estimate indicates that the decay region inside the vacuum tank should be kept at  $\approx 10^{-7}$  mbar to avoid significant backgrounds from the scattering of  $\pi^+$  on the residual gas. This is about hundred times better than the vacuum quality achieved running Na48/2 during 2004. Several tests are proposed to evaluate how to achieve the specified vacuum level.

- We will first check the ultimate vacuum which can be reached in the present configuration but without the Kevlar window. We will remove the Kevlar window and close the vessel using the available end-cap. This test can be carried as soon as we have access in the area. We have to remove the beam pipe between chamber 1 and 2, move chamber 1 downstream, remove the beam pipe between chamber 1 and the Kevlar window, remove the Kevlar window and install the end-cap. The vessel will be evacuated and the ultimate vacuum recorded.
- If a vacuum of  $10^{-7}$  mbar cannot be reached under these conditions, we will have to investigate different ways to improve it: better surface cleaning or coating, new seals, or getters. We plan to seek advice from the CERN/TS-MME group.

- We have also to improve the tightness of the Kevlar window for example using a thin aluminum liner, and a new beam pipe connection. These tests could be performed on the Kevlar window used until the incident in 1999 which is still tight.

## 4 Detectors

The detector elements are listed here together with a brief functional description. The principle elements are then described in the following sub-sections. A detector layout is shown in Figure 6.

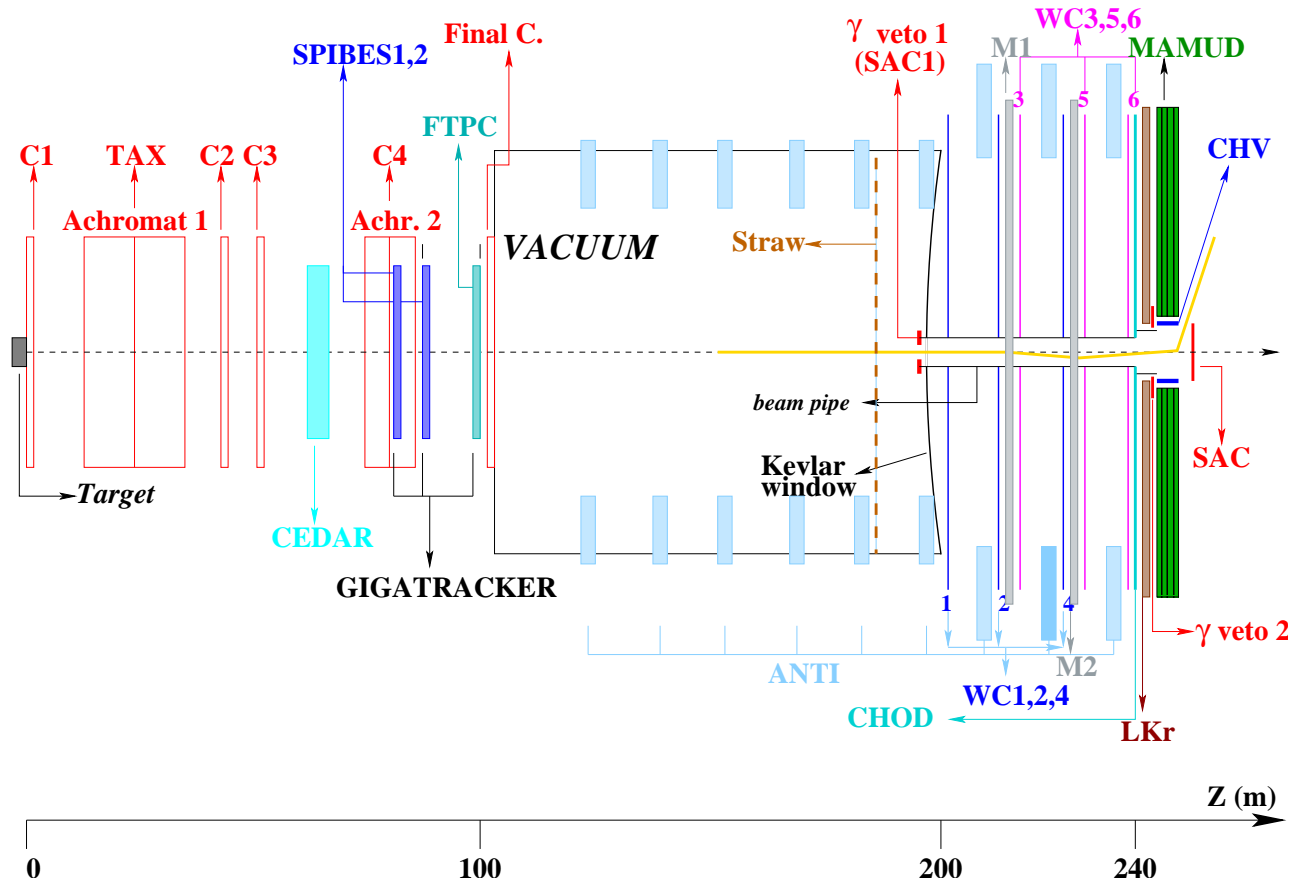


Figure 6: Detector Layout

### 1. CEDAR

A Differential Cherenkov counter (an upgraded form of the CEDAR built for the SPS secondary beams [16]) placed on the incoming beam to tag the minority particles of

interest (kaons).

## 2. GIGATRACKER

- FAST PIXEL (SPIBES)

Ultra-thin silicon micro-pixel detectors for (redundant) momentum measurement of the incoming beam with deep-sub-nanosecond time resolution to provide a tight time coincidence between the kaon and the pion tracks and to simplify the pattern recognition in the following gas TPC.

- Micromegas-based Flash-TPC (FTPC)

A gas Time Projection Chamber to measure the direction of the incoming beam particles with the least amount of material to minimise the effect of multiple scattering on the measurement of the angle between the kaon and the pion.

## 3. ANTI

A set of ring-shaped anti-counters surrounding the vacuum tank and providing coverage for photons originating from the decay region with angles larger than 15 mrad.

## 4. WC

A double magnetic spectrometer to measure the direction of the out-coming pion and its momentum and to provide a redundant measurement of the latter.

## 5. CHOD

A hodoscope for triggering and precise timing of the charged track.

## 6. LKR

A high-performance electromagnetic calorimeter acting as photon veto between in the angular region between 1.0 and 15.0 mrad. The baseline option is to re-use the NA48 Liquid Krypton Calorimeter (LKR) with properly updated electronics.

## 7. MAMUD

A magnetised hadron calorimeter and muon detector capable to identify muons with inefficiencies smaller than  $10^{-5}$ . It also serves the purpose of deflecting the charged beam away from the photon detector (SAC3) placed at the end of the hall.

## 8. SAC

Small angle photon vetoes covering the small angle beam pipe region which traverses the magnetic spectrometer

## 9. CHV

A charged-particle veto, incorporated in the beam-pipe of MAMUD, to provide hermetic coverage for charged particles coming from kaon decays and occupying the beam region.

## 4.1 CEDAR

The purpose of the CEDAR is to identify individual kaons positively. This is important because only a small fraction of the incoming beam particles are kaons. A beam pion undergoing a scattering in the residual gas contained in the decay tank may be mistaken as signal if no other visible particles are produced in the process. CEDAR counters were built for use at the SPS. The counter is crossed by a rate of particles up to 1 GHz. However, exploiting the dependence of the Cherenkov angle on particle speed, Cherenkov photons originating from pions can be blocked by a diaphragm and do not reach the photo-detectors. Cherenkov photons originating from protons miss the photo-detectors as well. The fraction of kaons is about 6%, so for a 1 GHz total rate, the counter should run at about 60 MHz. The divergence of the beam should not exceed 0.1 mrad. Details concerning the CEDAR can be found in [16].

## 4.2 GIGATRACKER

The NA48/3 experiment requires tracking with unprecedented characteristics. The particle rate per  $\text{cm}^2$  (40 MHz/ $\text{cm}^2$ , total rate up to 1 GHz) is only about a factor of two larger than that foreseen for the innermost pixel layer of the proton-proton experiment CMS at the LHC and is presumably manageable. However, the extremely limited material budget ( $\ll 1\% X_0$ ) and the required time resolution of less than 100 ps are technologically very challenging. The planned spectrometer is based on hybrid technology, with thin, fast silicon micro-pixel to provide a redundant momentum measurement to  $\approx 0.5\%$  resolution and bi-dimensional pattern recognition, plus a micromegas-based TPC, read-out by high speed FADC to provide the measurement of the incoming charged track direction.

Since the flux of protons that can be delivered by the SPS to the T10 target is not a limitation, the overall performance of the experiment will be directly coupled to the performance of the gigatracker. We call gigatracker the hybrid detector formed by the silicon pixel layers plus

the gaseous detector. The silicon pixel detectors are chosen to provide excellent time and position resolution.

State-of-the-art pixel assemblies (ALICE) deploy silicon sensors of  $200\ \mu\text{m}$  thickness coupled to  $150\ \mu\text{m}$  thick read-out chip. The PCB and bonding lead to an overall thickness of about  $1\% X_0$ , thus limiting the momentum resolution. Efforts must be made to reduce the read-out chip and overall thicknesses. The required position resolution of  $50\ \mu\text{m}$  can be achieved easily.

The Si pixel detector is a good candidate to achieve the required time resolution. The capacitance of a single pixel is typically  $100\ \text{fF}$  including the input capacity of a fast pre-amplifier and the stray capacitance to the neighbouring pixels.

A signal-to-noise ratio of 50 for minimum ionizing particles has been achieved with  $0.25\ \mu\text{m}$  CMOS process and for a  $25\ \text{ns}$  peaking time (Alice/LHCb). This project requires a rise-time of less than  $2\ \text{ns}$  which seems achievable using a more advanced  $0.13\ \mu\text{m}$  CMOS process (P. Jarron, private communication) with a signal to noise ratio that is still acceptable. It appears therefore feasible to reach a time resolution better than  $100\ \text{ps}$  for minimum ionizing particles. This has of course to be demonstrated by R&D and prototype testing.

In conclusion, since the Si-pixel detector seems an extremely promising option to achieve the stringent specifications of the NA48/3 experiment, we request that prototype function ASICs (pre-amplifier, discriminator and high resolution TDC) be developed for test in a high intensity particle beam. This preliminary study will then be followed by the design of a full-scale pixel ASIC. In the final design we expect to use the  $0.13\ \mu\text{m}$  CMOS process currently being investigated for HEP applications.

#### 4.2.1 The fast pixel detector: SPIBES

A silicon pixel beam spectrometer for the possible NA48/3 experiment has extremely demanding requirements, some of which are recalled below:

- Beam intensity  $\approx 4 \times 10^7\ \text{cm}^{-2}\text{s}^{-1}$
- Amplifier peaking time  $\approx 1\ \text{ns}$
- On-chip TDC resolution  $\approx 100\ \text{ps}$
- Radiation exposure total dose TID (estimation for 100 days operation)  $\approx 120\ \text{kGy}$  (=  $12\ \text{Mrad}$ )
- Fluence  $\approx 4.5 \times 10^{14}\ \text{cm}^{-2}$  (1 MeV neutron equivalent)

- Material budget as low as possible ( $\ll 1\% X_0$ )

These requirements raise major challenges and in particular require novel developments in some key technologies, such as deep submicron electronics, that have recently become available to the HEP community. The aim of this section is to outline a road map for the study of the problems and the implementation of the most effective solution within the time constraints of the start of the proposed experiment.

This section is written with the participation, on a personal basis, of some members of the ALICE silicon pixel detector collaboration (SPD) as well as some members of the PH-MIC Group at CERN. The SPD project has developed a complex front-end electronics in the currently most advanced  $0.25\ \mu\text{m}$  CMOS process, together with state-of-the-art techniques to match the severe constraints in material budget (wafer thinning, etc). An ALICE single assembly has recently been placed in the NA48/2 beam line for preliminary test runs at high beam intensity. General features of the detector and first results are reported later in this document. The CERN-PH/MIC group has been responsible for the design of the SPD pixel chip and is studying high speed designs that could be applicable to this project.

#### 4.2.2 Front-end Electronics and Sensors

##### 1. Pixel detector technology

The only pixel technology sufficiently mature for consideration in the time frame of the project is the one based on hybrid pixels. Each pixel consists consist of a readout chip bump-bonded to a sensor (generally silicon). Monolithic pixels have been investigated in recent years but have not yet reached a stage at which they could be considered as a realistic option. More recently a detailed study has been started of devices based on the deposition of a layer of amorphous silicon or other suitable material on the surface of a readout chip. Although promising results have been obtained, this technology is still in its infancy. Therefore it is proposed to focus the effort on hybrid pixels with thin silicon wafers and low mass hybrids. In the ALICE SPD, one of the most advanced current designs, pixel chips of  $150\ \mu\text{m}$  thickness (from thinned 200 mm diameter wafers) are bump-bonded to  $200\ \mu\text{m}$  thick Si sensors. To reduce further the material budget, bump-bonding of even thinner silicon elements is required and needs to be investigated.

##### 2. Silicon sensors

Sensor thickness will have to be optimized taking into account the trade-off between speed and collected charge for different designs. Detailed simulations and direct mea-

measurements are required. Sensor wafers of thickness  $\leq 150\mu\text{m}$  can be obtained from commercial suppliers but production and bump-bonding yield need to be investigated; this work could start immediately using available pixel chips. Radiation hardness is another critical issue to be studied; the experience gained in the development of Si tracking detectors for the experiments at the LHC will be very valuable. To achieve 100 ps time resolution seems feasible with advanced 130 nm CMOS if 90% of the charge detected by the sensor is collected within 1 ns, which is far from obvious. Therefore, an intense effort should be done to investigate the high speed silicon sensor.

### 3. Pixel chip

The pixel chip will be a mixed-signal ASIC of very high complexity. The chip architecture will require a detailed study and thorough simulation. The most challenging functional blocks will be:

- (a) very fast preamp and shaper
- (b) very low time walk discriminator, and
- (c) high resolution TDC.

A preliminary design of each block will be done in the  $0.25\ \mu\text{m}$  process using Multi Project Wafers (MPW) runs for cost considerations. For the full design, the speed and device density requirements will surely need moving to the  $0.13\ \mu\text{m}$  process. The study of this technology has started very recently and the design of such a complex structure is expected to require an effort of several man-years.

### 4. Front-end hybrid

In the current designs the pixel chips are placed on a substrate carrying power distribution, signals and data buses. The substrate is a low-mass multilayer flex, such as polyimide/aluminium. In addition to the pixel chip, additional FE electronics functionality is needed for clock and trigger distribution, data multiplexing and transmission, and controls. This requires one or more ASICs in the immediate vicinity of the pixel chips, possibly on the same substrate. This results in a front-end hybrid, or multi-chip-module (MCM). It is a complex and challenging design on which considerable experience has been gained in the developments of the Si trackers for the LHC experiments. For this project, it would be desirable to have the power, data buses and the MCM functionality placed at the periphery of the detector plane, in order to minimize the material budget. The feasibility of such a scheme needs to be investigated,

including the implications for cooling. It might also be possible to take advantage of deep via in silicon, a novel process currently under study, which could lead to a further reduction in material.

#### 5. Mechanics and cooling

The power dissipation in the pixel chip may reach  $\approx 2\text{W}/\text{cm}^2$ , possibly more on account of the very high speed required. An efficient cooling system is mandatory. This is of course not easily compatible with the low mass requirements. It is planned to study the feasibility and performance of thin substrates consisting of high thermal conductivity carbon fibre composites, cooled at the periphery to reduce the material to the minimum. Expertise has been gained in the ALICE SPD on composite materials and two-phase cooling systems. Other advanced technology solutions, such as microchannel cooling, are being developed elsewhere and might be considered if compatible with the detector layout.

#### 6. Timescale and resources

The preliminary time scale has been established, based on the experience gained in other silicon pixel detector projects. The baseline technologies are essentially those already adopted in the most advanced current designs, further extended to the limits of feasibility. The pixel chip will probably require developments in the  $0.13\ \mu\text{m}$  CMOS process. Novel solutions may have to be worked out for the hybrid and cooling. Preliminary work should start without delay, particularly on the definition and simulation of the front-end architecture. The front-end ASIC development will require the contribution of several experienced designers for a period of two to three years. Testing is a key activity that requires a close collaboration of physicists and designers. A good definition of the DAQ environment is needed to develop a matching back-end readout and an efficient calibration system.

### 4.2.3 Micromegas-type TPC

The multiple scattering caused by material of the last tracking station of the gigatracker impacts directly on the angular resolution in the measurement of the opening angle between the kaon and the charged pion and hence it has to be minimised. The state-of-the-art gaseous detector developed for NA48/2 couples very good space resolution to a minimal material budget. The NA48/2 detector, called KABES, is made of MICROMEGAS-type chambers read-out in TPC mode. They have achieved very good performance [15], [21].

- Position Resolution  $\approx 80 \mu\text{m}$
- Time resolution  $\approx 0.7 \text{ ns}$
- Rate per micro-strip  $\approx 2 \text{ MHz}$

In NA48/3 a similar detector has to be able to perform the tracking of a 1 GHz hadron beam (about 10 times more intense -per unit area- than the combined positive and negative beams of NA48/2), contributing less than  $10 \mu\text{rad}$  to the angular resolution. Effort has to be made to:

- Shorten the detector signal employing a micro-mesh with thinner amplification gap.
- Improve the time resolution which is currently 0.7 ns.
- Reduce the double pulse resolution, sampling each strip continuously by means of 1 GHz FADC.
- Consider a smaller micro-strip pitch.

Another aspect that has to be taken into account is the space charge effect due to ion build-up. The design of the experiment relies on the ability of the KABES detector to function at the required intensity. To a large extent this was already validated in 2004 during the test which took place at the end of the NA48/2 data taking as described in Section 9.

For NA48/3 this gaseous detector is dubbed Flash-TPC because, in order to achieve the required double pulse resolution to make the pattern recognition feasible in a detector without intrinsic bi-dimensional segmentation, each micro-strip will be read by FADCs of the type or similar to those employed for the proton tagger of the original NA48 experiment. The pattern recognition is complicated by the long drift time (about 600 ns) and the time resolution is unlikely to reach 100 ps because of gas diffusion. For these two reasons the FTTPC is preceded by a fast pixel detector (SPIBES).

### 4.3 ANTI

These are a set of ring-shaped anti-counters surrounding the vacuum tank and providing full acceptance for photons originating from the decay region with angles larger than  $15 \text{ mrad}$ . NA48 is equipped with photon vetoes with the appropriate coverage. The design for NA48 was based on a 35 mm iron / 10 mm scintillator sandwich repeated twice. The inefficiency due to punch-through photons was of the order of  $10^{-2}$  and even a modest modification of the

present configuration would not allow to reach the required rejection factor needed for the new experiment. The importance of ANTI is discussed in Section 8 where the suppression of backgrounds coming from the decay  $K^+ \rightarrow \pi^+\pi^0$  is outlined and the tolerable inefficiency for the various photon detectors is defined. To achieve the necessary rejection of  $\pi^0$  coming from the  $K \rightarrow \pi^+\pi^0$  reaction, the single photon veto inefficiency in the angular region covered by the ANTI must not exceed  $10^{-4}$  for photons with energies larger than 100 MeV. To achieve the above performance it is necessary to consider two contributions to photon inefficiency: 1) punch-through; 2) photonuclear interactions. In this context we ignore the contribution due to the leakage through the cracks: indeed we assume that the counter layout will be optimized to minimize that source of inefficiency. We remark that while the contribution due to the punch-through can be precisely calculated with EGS or GEANT, the photo-nuclear component requires more careful study. On the experimental side there have been only two measurements from E787 [22] and from ES-147 and ES-171[23]. E787 selected  $K_{\pi 2}$  candidates measuring the  $\pi^+$  and one of the two gammas and predicting the other, while the technique developed by the ES experiments used tagged photons from an electron beam. The range of energies probed by the two groups was somewhat complementary: 20 - 220 MeV for E787 and 185 - 505 MeV for ES-147. The veto structure was a sandwich of Pb-scintillator with the Pb converter thickness ranging between 0.5 to 2.0 mm. A comparison of the results is rather difficult because the details of the experimental setup were different. However both agree that the veto inefficiency from the photonuclear component is around  $10^{-4}$  for a threshold on the visible energy set at 1 MeV. We add that the ES group studied also a veto wall made of CsI crystals and with this configuration they found an inefficiency which was an order of magnitude smaller than for lead/scintillator sandwich. Following the experimental studies performed by these groups one can conclude that, with a fine sandwich of lead (1-2 mm) and plastic scintillator (5 mm) the resulting photon veto inefficiency matches the requirements of  $10^{-4}$ . To optimize further the design we have initiated a study based on GEANT4. Simulation and experimental data are in fair agreement, but some adjustment of the simulation of the secondary production might be necessary. With this tool we plan to finalize the Lead/Scintillator segmentation.

#### 4.4 Wire Chambers (WC)

To provide a redundant measurement of the momentum of the outgoing pion, we are planning to use a double magnetic spectrometer. Two new chambers need to be built. A copy of the MNP33 dipole magnet which is currently employed by NA48/2 will be required. The

NA48 spectrometer is formed by 4 large drift chambers. Their behaviour at the kaon decay intensity proposed for the new experiment ( $\simeq 10$  MHz) was tested during the last week of NA48/2.

The material of the first tracking station affects the measurement of the angle between the incoming kaon and the outgoing pion in a way similar to the last tracking station of the gigatracker. For this reason every effort has to be made to minimise the multiple scattering due to the material crossed by the particles. The NA48 drift chambers are housed in a stainless steel vessel full of helium because they need to operate at near atmospheric pressure. The decay vacuum tank and the helium tank are separated by a thin window made of Kevlar, about 1 mm thick, corresponding to about 0.3 %  $X_0$ . In this setup, the window, the first drift chamber and the helium between the first and the second chambers all contribute to the deterioration of the angular measurement.

A possible way to improve the angular resolution is to employ a detector able to operate in vacuum upstream of the Kevlar window. A straw tracker based on the technology developed for example for the ATLAS TRT may be a viable solution and is being investigated. Straws have been used in precision rare kaon decay experiments [24].

A more elegant solution would be to replace all the current drift chambers with straws, to eliminate the beam pipe and the Kevlar window and to extend the vacuum up to the charged hodoscope. It is worth mentioning that the current NA48 helium tank is a certified vacuum vessel and was used as such during the year 2000 when the drift chambers, damaged by the implosion of the beam pipe, were removed and the vacuum was extended to the He tank region. The Dubna Laboratory has significant experience with straw trackers having been involved in the construction of the ATLAS TRT end-cap and of the large-size straws for the COMPASS experiment.

Another advantage of straws with respect to the more conventional NA48 drift chamber design is the shorter drift time which make them a better detector for the high rates of NA48/3. Given the small diameter of the straws (e.g. 4 mm in the case of ATLAS) their operation in a vacuum vessel should not pose particular concern [25]. Issues related to outgasing, leak rate and the development of appropriate gas fittings, signal and high voltage feed-throughs have to be investigated for the straw-based option.

## 4.5 CHOD

The charged hodoscope is used to provide a fast trigger and, together with the upstream fast detector (gigatracker) and the differential Cherenkov (CEDAR), is used to provide a tight

time coincidence between the incoming kaon and the  $\pi^+$ . This task is performed off-line to guarantee as far as possible that the event is not due to a charged track accidentally associated with an independent incoming particle. Since the  $K^+$  decay rate is of the order of 10 MHz and the rate of beam particles is about 800 MHz, of which 50 MHz are kaons, the detector must have good intrinsic time resolution, better than 100 ps. This will guarantee that the probability of having two Kaons in the unresolved time window is below 1%, which, for a quite reasonable "double K" resolving inefficiency of 2% provided by the CEDAR, gives rise to an accidental mistagging probability of the order of  $2 \times 10^{-4}$ , similar to the expected kinematical rejection factor.

To build the hodoscope (about  $2.5 \times 2.5 m^2$ ), we are considering various possibilities, such as

- to look at the light produced by a scintillator orthogonal to the beam axis, using PMs just behind it, in order to minimize the light path to a few centimetres. With this solution, the number of fast Photo-Multipliers (PM) needed is around 2000;
- to use fused silica instead of scintillator and to look at the Cherenkov light, in order to minimise the light time dispersion. In this case, however, we need to incline the quartz slab at around 45 degrees with respect to the beam axis, in order to obtain a light output from it <sup>||</sup>. In this case, the number of PMs is higher but should not exceed 3000.
- to use a Multigap glass RPC, for which the ALICE Collaboration has obtained time resolution down to 50 ps with rates up to 1 KHz/  $cm^2$ . However, this option will require further studies since, in the hottest region near the beam pipe, the rate measured in the recent tests at close to the future nominal intensity was about 5 kHz/ $cm^2$ .

Since the hodoscope is just in front of the LKr calorimeter, in principle it might spoil its resolution and its photon detection efficiency. For this reason one of the important issues to be considered is the amount of material that will be needed, as well as its uniformity. We have collected data using prototypes for solutions i) and ii) and results should soon become available.

---

<sup>||</sup>For a slab orthogonal to the beam, internal total reflection prevents the light to escape in air and we would need proper optical matching

## 4.6 LKR

The natural choice to detect photons in the forward angular region is to employ the existing NA48 Liquid Krypton Calorimeter (LKR). The very good energy resolution of this calorimeter is not strictly necessary for the new experiment but represents an asset to study radiative decays and other rare kaon decays that can be measured with this setup. However, the most important question to answer is whether the LKR is a good choice for the function it has to perform in the new experiment, that is to achieve an inefficiency smaller than  $10^{-5}$  in vetoing photons with energies larger than 1 GeV.

The advantages of employing the NA48 calorimeter are:

1. It exists
2. Very good granularity:  $2 \times 2 \text{ cm}^2$
3. Very good energy resolution:

$$\frac{\sigma(E)}{E} = \frac{3.2\%}{\sqrt{E(\text{GeV})}} \oplus \frac{9\%}{E(\text{GeV})} \oplus 0.42\% \quad (7)$$

4. Very good time resolution:  $\approx 300 \text{ ps}$  for each photon
5. It is a quasi-homogeneous ionisation calorimeter

The disadvantages are:

1. The passive material in front of the active liquid krypton amounts to about  $0.5 X_0$ .
2. It is a cryogenic detector requiring maintenance and operation of a control system.

### 4.6.1 LKR Control System

The control system consists of 3-levels:

- Sensors
- Front Ends (main control)
- Supervision (human interface)

As we assume that all existing sensors will be reused for the future operation they will not be discussed here.

- Front End Hardware

The Front End hardware was built using SIEMENS PLCs (models: S5-115U, S5-135U, and redundant S5-115H and S5-155H) about 10 years ago. The PLC's need periodic maintenance (which is not very time consuming) but otherwise they have run without problems for more than 8 years. The hardware is robust and capable to run another 10-15 years. Although expensive, spare parts are available from SIEMENS.

- Front End Software

The Software is written in the S5 language. It was developed and well documented at CERN mainly by J.P.Orlic who would need to be replaced. In the longer term, the S5 based system will be obsolete and will become more difficult to maintain. It should be noted that the CERN-developped cryogenic control framework UNICOS (UNified Industrial COntrol System) does not support the old PLC models.

- Supervision system

The system uses a HP station running UNIX. The station is rather robust and it has run without problem during the last few years. There are few spare stations. The software was developped at CERN, it is based on a commercial package FactoryLink. The list of available spares from HP is limited. There is no longer any CERN-wide support for the HP, UNIX and FactoryLink. UNICOS supervision is based on PVSS running on PC.

In conclusion, in order to operate the LKR control system, the following actions have to be taken as soon as possible.

1. Find a replacement for J.P.Orlic before the end of 2004
2. Decide whether we should:
  - keep the existing PLCs (expert will be needed)
  - upgrade to modern PLC's and UNICOS (money + manpower for development)
3. Move the supervision to PC and PVSS (manpower mainly )

## 4.7 MAMUD

To provide pion/muon separation it is planned to install a new magnetised hadron calorimeter and muon veto (MAMUD) behind the Liquid Krypton (LKR) calorimeter. The design

consists of magnetised iron plates which create a dipole field of about 1.5 T in the beam region in order to deflect the beam away from the small-angle photon veto counters (SAC) installed at the end of the hall on the detector axis. A sketch of the hadronic calorimeter is shown in Figure 7.

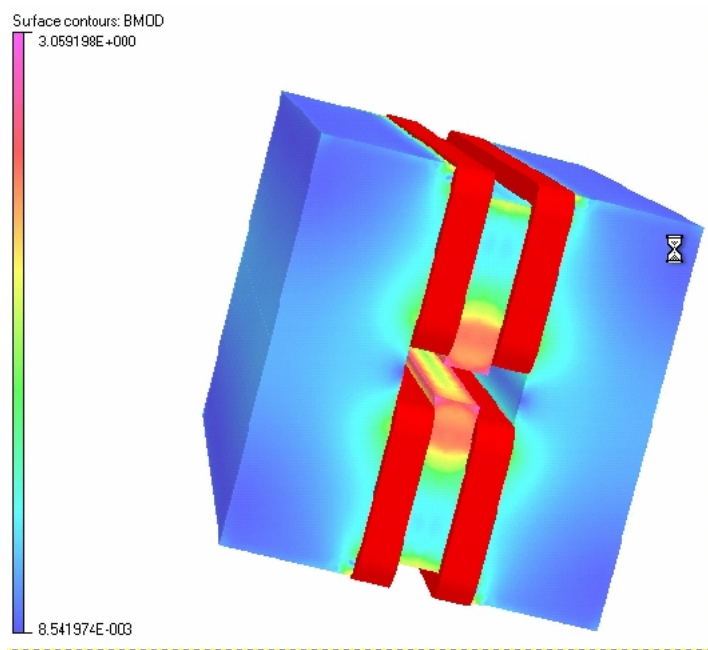


Figure 7: Sketch of the hadron calorimeter (MAMUD). The iron lamination is not shown.

The magnetic field is generated by four coils. The fields generated by the two upper (or lower) coils have opposite directions, so there is a vertical field across the 22 cm gap. The diameter of the beam tube is increased from 16 to 21 cm at the exit of the LKr calorimeter, so that small-angle photons from  $\pi^0$  decay traversing the LKr calorimeter inside the beam tube continue to travel in vacuum until they hit the small-angle photon veto counters at the end of the hall.

The iron of the hadronic calorimeter is subdivided into 150 plates, each 2 cm thick, with a gap of 1.5 cm between consecutive plates. The total length of the calorimeter is 525 cm, and the cross-section of the sensitive volume (excluding the central hole) is  $260 \times 260$  cm. The active detector material consists of strips of extruded polystyrene scintillator, 4 cm wide, 130 cm long and 1 cm thick, which are inserted in the gaps between plates. The scintillation light from each strip is collected by wavelength-shifting fibres with a diameter of 1.2 mm which are glued in a groove along the strip length.

This technique has been adopted by the MINOS and OPERA experiments. Tests performed

by the MINOS collaboration on 8 m long strips have shown that a minimum ionizing particle crossing the strip at a distance of 130 cm from its end produces a signal corresponding to 4.5 photo-electrons at the cathode of a photomultiplier tube (PMT) optically connected to the wavelength-shifting fibre glued to that strip. The strips of two consecutive planes will be oriented in orthogonal (horizontal or vertical) directions in order to provide two-dimensional shower information.

We propose to subdivide the calorimeter longitudinally, starting with three independently instrumented sections of 17 iron plates each, corresponding to  $\approx 25 X_0$  and 2 absorption lengths for hadronic interactions. This is similar to the thickness of the LKr calorimeter. Gaps 52 through 132 are purely passive, while the last 17 gaps are again instrumented to provide additional rejection for muons which have undergone "catastrophic" energy losses in one of the first three sections.

In both MINOS and OPERA the scintillator strips are read out individually, using multi-anode PMs, to provide simultaneous tracking and calorimetric information. In our case this is not necessary, and we plan to group several consecutive strips onto a single PM. A minimal scheme consists in connecting nine consecutive horizontal (or vertical) strips to a single 1 cm diameter PM. In such a scheme, and with the longitudinal segmentation described above, the total number of 1 cm diameter PMs is 1040, for a total scintillator area of  $\approx 460 \text{ m}^2$ .

With a magnetic field of 1.5 T, the calorimeter provides a  $p_T$ -kick of 1.35 GeV/c, deflecting the beam laterally at the end of the hall by 16 cm. This should be sufficient for a safe operation of the small-angle photon veto (SAC3).

The longitudinal segmentation of the hadron calorimeter, together with its transverse granularity of 4 cm, is crucial to identify and reject "catastrophic" energy losses of muons from  $K^+ \rightarrow \mu^+\nu$  decay. With the exception of deep-inelastic muon - nucleon scattering ( $\mu + N \rightarrow \mu + \text{hadrons}$ ), all "catastrophic" muon energy losses, including muon decay, produce a single electromagnetic shower which can easily be distinguished from a hadronic shower by its lateral and longitudinal size. In addition, with the exception of muon decay, after suffering a "catastrophic" energy loss the muon itself has generally enough residual energy to be identified as a single minimum-ionizing particle in the other instrumented sections of the calorimeter. Even in the case of muon decay, the decay electron generally has only a fraction of the muon momentum, resulting in a measurable inconsistency between the momentum, as measured in the spectrometer, and the shower energy.

Detailed simulations are needed to optimize the design of the hadron calorimeter and to assess its rejection power against muons from  $K^+ \rightarrow \mu^+\nu$  decay. We note that the response

of the hadronic calorimeter, as well as that of the LKr calorimeter, can be studied "in situ" with high statistics by deflecting beams of pions and muons of variable momentum into the calorimeter by means of small steering magnets located just before the beginning of the decay volume. This technique, which has been used successfully in NA48/2 for calibration purposes, will provide a measurement of the muon rejection power.

## 5 Trigger

As is indicated in Table 4, the single particle rate in the detector is dominated by the kaon decays. Although we plan to use only the first 50 m after the final collimator as fiducial region, for the trigger rate estimates we must consider all decays happening in the vacuum tank upstream of the main detectors. This leads to an input rate of 10 MHz kaon decays which, owing to the uniform nature of the slowly extracted SPS beam, occur without a time structure. In other words, kaon decays happen without a minimal time interval between them. The rate mentioned above, already assumes an effective spill length of 3 s for a 4.8 s flat top, as suggested by the NA48/2 experience. In Table 5 the main  $K^+$  decays are listed together with the detector elements that will be employed in the trigger to suppress them.

Decay Mode	Detectors used for Rejection
$K^+ \rightarrow \mu^+\nu$	MAMUD, WC, CHOD
$K^+ \rightarrow \pi^+\pi^0$	CHOD, ANTI, LKR, SAC
$K^+ \rightarrow \pi^+\pi^+\pi^-$	CHOD, WC, CHV
$K^+ \rightarrow \pi^+\pi^0\pi^0$	CHOD, ANTI, LKR, SAC
$K^+ \rightarrow \pi^0\mu^+\nu$	MAMUD, ANTI, LKR, SAC
$K^+ \rightarrow \pi^0e^+\nu$	MAMUD, ANTI, LKR, SAC

Table 5: Detectors used to reject the main  $K^+$  decay modes.

It is important to reduce the rate as much as possible with simple trigger cuts in order to avoid correlations between the different sub-detectors. About 2/3 of the  $K^+$  decays contain a muon in the final state so the use of MAMUD as muon veto in the trigger will be essential. The ANTI detectors will be used in veto to reduce the rate due to  $K^+ \rightarrow \pi^+\pi^0$ . We expect that the rate of kaon decays passing the MAMUD and ANTI veto conditions will be about 1/4 of the initial one, or 2.5 MHz.

Further rejection will be provided by the detection of electro-magnetic showers in the LKR.

To fully exploit the fine granularity of LKR (the towers have a  $\sim 2 \times 2$  cm<sup>2</sup> cross-section) a truly bi-dimensional and pipelined trigger processor should be envisaged. At the time when the NA48 LKR pipelined trigger was designed (1992) a bi-dimensional trigger was too complex to be proposed. Now, building on the experience of the LHC experiments and the technological advances, it should be affordable. The trigger will be used to count electro-magnetic showers in the calorimeter and to veto events with more than one cluster. Combining the LKR criteria with the vetoes will reduce the rate to about 1 MHz. The CHOD will be used to provide a fine time reference for the trigger and to veto events with more than one charged track. Further suppression will rely on the use of the wire chambers. To reject events with more than one charged track, multiplicity cuts based on the number of hit wires in each wire chamber (WC) can be applied. All the criteria mentioned above, possibly coupled to veto requests in the SAC and CHV detectors, will reduce the rate to allow a processor-based trigger system to analyse the WC information and to apply mild cuts on the event missing mass. This last cut will comfortably take the rate down to a frequency and data size manageable by Higher Level Triggers housed in a PC farm. Two points should be stressed. About half of the trigger band-width will probably be reserved to collect down-scaled triggers where far less stringent trigger conditions will be applied. These relaxed samples will be used to study the correlations between different analysis cuts. Ancillary triggers may also be added to collect less rare but still very interesting  $K^+$  decays.

## 6 Electronics, Data Acquisition and DCS

The existing NA48 Detector Control System (DCS) was developed by CERN about 10 years ago and is now obsolete. It has to be upgraded applying new technology supported at CERN and recommended by IT/CO, using Windows and Linux PCs as hardware. The supervision of the new system can be built using PVSS SCADA product and developed by IT/CO JCOP framework. The Front End layer should be based on commercial OPC servers as much as possible. We are presently considering the ELMBs designed by the ATLAS Collaboration as the most cost effective solution for analog measurements. Most of the NA48 existing sensors and cables can be reused for the new experiment, thereby reducing considerably the cost of the upgrade.

## 7 Suppression of the $K^+ \rightarrow \pi^+\pi^0$ Background

The purpose of this section is to show which photon detection inefficiency can be tolerated in order to suppress the backgrounds from the decay

$$K^+ \rightarrow \pi^+\pi^0 \quad (8)$$

to the  $K^+ \rightarrow \pi^+\nu\bar{\nu}$  interesting signal by about 8 orders of magnitude. Since any further reduction of the background from reaction (8) must exploit the two body kinematics, it is important to keep the photon veto and the kinematical rejections as independent as possible. In a toy simulation, a monochromatic beam of positively charged kaons with momentum of 75 GeV/ $c$  and directed along the detector axis are made to decay into  $\pi^+\pi^0$ . Two photon rejection situations are analysed:

- **A:** No cut on the  $\pi^+$  momentum

In this situation one tries to veto all photons from the background reaction without assuming that the  $\pi^+$  track is correctly measured. In this way the factorization (i.e. independence) of the photon veto and kinematical rejections is preserved. It will be shown that, in order to achieve the specified  $\pi^0$  rejection, the requirements on the photon detection efficiency are very tight.

- **B:** Cut on the  $\pi^+$  momentum

The momentum  $p_{\pi^+}$  of the outgoing charged pion is required to satisfy the relation:

$$8 \text{ GeV}/c \leq p_{\pi^+} \leq 40 \text{ GeV}/c \quad (9)$$

In this case the requirement on the capability of the photon vetoes can be relaxed but one has to take into account the correlation with the charged track momentum mis-reconstruction. For example if a 65 GeV/ $c$  pion is misreconstructed as a 35 GeV/ $c$  particle, one may be misled to interpret the event as signal because the photon veto rejection for a  $\pi^0$  of *presumed* momentum  $p_{\pi^0} = 75 - 35 = 40 \text{ GeV}/c$  is supposed to be good enough to reduce the background to the required level.

There is a strong correlation between the energy and polar angle of the photons emitted from the  $\pi^0$  decay. For the actual design of the experiment, we will fold the longitudinal distribution of kaon decays into the detector acceptance. Why does one need a  $\pi^0$  rejection factor of  $\simeq 10^8$ ? This number is obtained as follows: the experiment aims to measure 100

Class	Polar angle	
1	0 – 1 mrad	Small Angle Calorimeters (SAC)
2	1 – 15 mrad	Typical LKr acceptance (LKR)
3	15 – 30 mrad	Large Angle Vetoes (ANTI)
4	30 – 100 mrad	Large Angle Vetoes (ANTI)
5	100 mrad – $\frac{\pi}{2}$	
6	$\geq \frac{\pi}{2}$	Photons going Backwards

Table 6: The angular regions used in the simulation.

$K^+ \rightarrow \pi^+ \nu \bar{\nu}$  events for a Branching Ratio  $BR \simeq 10^{-10}$  and a background not larger than 10% of the signal. With a 10% signal acceptance, 100 signal events require  $10^{13}$  decays in the fiducial volume. With  $BR(K^+ \rightarrow \pi^0 \pi^+) \simeq 0.2$ , and allowing for no more than 10 background events in the final sample, the overall rejection factor for this background amounts to  $2 \times 10^{11}$ . As already stated, reaction (8) is characterised by two-body kinematics and it is plausible that this constraint will allow background to be rejected by a factor of a few thousand once the requirement of consistent measurement of the  $\pi^+$  momentum by both magnetic spectrometers is made. This leaves a background rejection of about  $\simeq 10^8$  to be achieved by vetoing either of the two photons. The design of the whole photon veto system requires an optimised choice of detector technology. Given the large NA48 investment in the high precision Liquid Krypton electro-magnetic Calorimeter (LKR), it is compelling to evaluate it as photon veto. The main limitation of the LKR as photon veto is that it cannot reliably detect photons with energies smaller than 1 GeV. It is therefore essential to clarify in which angular region the LKR represents a viable option for the experiment. To study the correlation between the angles of the two photons, the angular coverage has been subdivided into six classes as outlined in Table 6.

The method to evaluate the tolerable inefficiency is as follows: the decays are binned in a  $6 \times 6$  matrix according to the polar angle of the two photons. An inefficiency is associated with each angular class. The background is estimated by summing over the  $6 \times 6$  classes and weighting them by the product of the inefficiency assumed for each class. No geometrical (acceptance) cuts are made. Ten million events were generated. The events are distributed in the  $6 \times 6$  matrix according to Table 7 for selection A. The events surviving the  $\pi^+$  momentum cut (Situation B) are displayed in Table 8. Values for the assumed inefficiencies are given in Table 9. The number of events expected in each class in units of  $10^{-10}$  is given in Table 10 for situation A and in Table 11 for situation B. The introduction of a momentum cut

Class	1	2	3	4	5	6
6	1	91				
5	227	42727				
4	2177	408102	6442			
3	7439	975678	165844	6334		
2	216289	6518116	974371	408080	42279	119
1		215809	7431	2225	219	

Table 7: Situation A: Distribution of the 10 million  $K^+ \rightarrow \pi^+\pi^0$  generated events.

Class	1	2	3	4	5	6
6		10				
5	15	4029				
4	169	41646				
3	867	152594				
2	166641	4405509	152555	41639	3917	17
1		166527	877	172	8	

Table 8: Situation B: Distribution of the  $K^+ \rightarrow \pi^+\pi^0$  events surviving the  $\pi^+$  momentum cut described in the text.

Class	Assumed Inefficiency	Minimum photon Energy (GeV)
1	$10^{-4}$	6
2	$10^{-5}$	1
3	$10^{-4}$	0.25
4	$10^{-2}$	0.02
5	1.	–
6	1.	–

Table 9: Assumed Inefficiencies.

Class	1	2	3	4	5	6
<b>6</b>	0.1	0.9				
<b>5</b>	22.7	427				
<b>4</b>	2.2	40.8	0.64			
<b>3</b>	0.074	0.98	0.17	6.3		
<b>2</b>	0.22	0.7	0.01	40.8	423	1.2
<b>1</b>		0.22	0.074	2.2	21.9	

Table 10: Situation A: Backgrounds in units of  $10^{-10}$  after photon rejection but before kinematical rejection. The total amounts to  $992 \times 10^{-10}$  which corresponds to a rejection power of about  $10^7$ .

Class	1	2	3	4	5	6
<b>6</b>		0.1				
<b>5</b>	1.5	40				
<b>4</b>	0.17	4.2				
<b>3</b>	0.009	0.15				
<b>2</b>	0.17	0.4	0.15	4.2	39	0.2
<b>1</b>		0.17	0.009	0.17	0.8	

Table 11: Situation B: The Total background after momentum cut, photon rejection but without two body kinematics rejection amounts to  $91.4 \times 10^{-10}$  corresponding to a rejection power of about  $10^8$ .

dramatically relaxes the tolerable inefficiency for the photon veto at the cost of potential correlation between the photon veto and kinematical rejection.

## 8 Preliminary Results from the 2004 Beam Test

It was of the utmost importance to test already in 2004 the performance of the NA48 detectors at intensities comparable to the NA48/3 ones, and to validate our (Monte-Carlo) knowledge of the photon vetoes with beam data. The availability of the charged kaon beam of NA48/2 which could be tuned to have characteristics comparable to those of NA48/3, offered a unique opportunity to quantify the necessary effort (technical and financial) to transform NA48/2 into a rare decay experiment capable of measuring  $K^+ \rightarrow \pi^+ \nu \bar{\nu}$ . Thanks to the extension granted by CERN to the 2004 NA48/2 running, we could devote a few days to these tests and we have indeed collected data to address the following issues:

1. Drift Chambers (WC)

We tested the NA48 drift chambers in conditions similar to those expected in NA48/3 with intensities up to a factor of 30 larger than NA48/2.

2. Gigatracker

- A state-of-the-art Si micro-pixel detector (ALICE/SPD) was used to familiarise us with the performance of such devices in the NA48/2 beam.
- A new micromegas micro-mesh with 25  $\mu\text{m}$  thick amplification gap allowed the pulses from the chambers to be shortened in order to reduce the occupancy of the TPC.
- The read-out of about 20 micro-strips of the current NA48/2 KABES detector by means of 480 MHz FADCs was used to measure the time resolution and the double pulse resolution. The FADCs were available from the read-out of the NA48 proton tagger during the  $\epsilon'/\epsilon$  measurement.

3. Photon Hermeticity

We complemented the NA48/2 setup with a small angle photon veto and collected a large sample of  $K^+ \rightarrow \pi^+ \pi^0$  decays with a minimum bias trigger to measure the  $\pi^0$  rejection power of the current setup and to extrapolate to the requirements of NA48/3.

4. We tested two prototype elements for the Charged Hodoscope (CHOD)

To perform the tests mentioned above, we requested one week of protons in the K12 beam line in addition to the time scheduled for NA48/2 during 2004. The data will be very important to proceed in due time towards a proposal. The data taking conditions and some very preliminary results are presented in the following subsections.

## 8.1 Drift Chambers (WC)

The K12 (NA48/2) beam rate of  $K^+$  decays was increased up to a factor of 30 with respect to the standard NA48/2 conditions by means of the following operations:

1. Opening up the aperture of the P42 proton beam line.
2. Tuning the K12 beam to  $+75 \text{ GeV}/c$ .
3. Opening up the momentum bite from  $\Delta p/p = 5\%$  to  $\Delta p/p = 20\%$
4. Turning on both beams of the present  $K^+$  and  $K^-$  line.
5. Employing a shorter T4 target (100 mm Be instead of 300 mm Be) in order to transport more protons on the experiment T10 target.

With the exception of one sector in DCH 3, Y view, all the other chambers could be operated at the highest beam intensity. A comparison of the tracking efficiency per plane at low and high intensity is shown in Figure 8.

The preliminary results are quite encouraging: the decrease of plane efficiency at the highest intensity is limited to about 1%. While the reason for this drop has still to be investigated, the ability to operate the chambers at intensities very close to those planned in NA48/3 cannot be overemphasised.

## 8.2 The NA48/2 KABES Detector

The KAon BEam Spectrometer (KABES) implemented in NA48/2 during 2003 [21] is taken as starting point for the gaseous station of the NA48/3 gigatracker. This detector is based on the Time Projection Chamber (TPC) principle and the amplification of the ionization signal is achieved by using Micromegas devices. The performance of KABES is found to be excellent in high-intensity hadron beams. The achieved space resolution of  $\sim 100 \mu\text{m}$  provides a measurement of track momentum with a precision better than 1% and the time

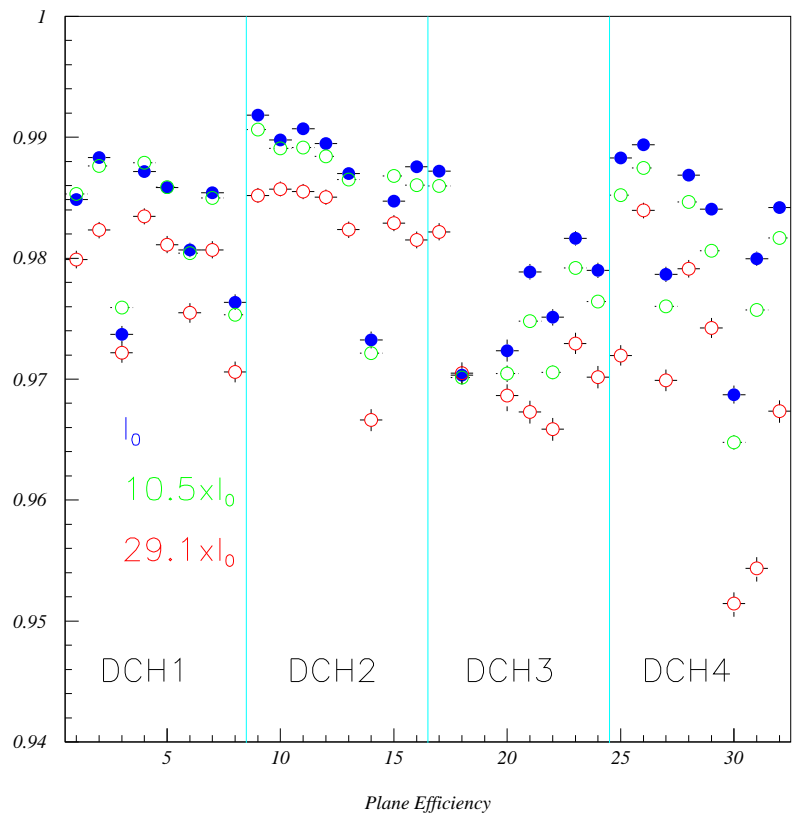


Figure 8: Comparison of WC efficiency per plane for different beam intensities.

resolution, better than 1 ns, allows the charged kaons in NA48/2 to be identified with almost no ambiguity. In the NA48/2 experiment layout, KABES is located along the charged kaon beam line, to measure precisely the direction and momentum of each particle. This spectrometer makes use of two stations separated by 8 m, in which small TPCs provide measurements of the transverse coordinates of the charged tracks.

The efficient detection and accurate measurement of the charged particle tracks in the high intensity beams rely on both the Micromegas and TPC techniques, the latter permitting the mesh to be positioned outside the high intensity region covered by the beam spot. To minimize the amount of material in the beam, two TPC-type detectors are used along the beam axis with opposite electric fields perpendicular to the track direction. The longitudinal depth of the detector is kept as small as possible in order to minimise multiple scattering in the various materials (0.13 %  $X_0$ ).

### 8.3 Performance of KABES with TDC read-out

The KABES pulses come from the front-end preamplifier and are transported for digitization to high performance TDCs [27] developed at CERN. For each signal detected on the strips by the front-end circuit, the discriminator senses the leading and the trailing time. The time over threshold ( $ToT$ ) of the signal represents the width of the ionization pulse. These  $ToT$  quantities provide crude but valuable information about the amplitudes needed to measure the vertical cluster position with the weighted strip coordinates while the horizontal position is derived from the drift time measurement.

The KABES read-out is designed to work at an input rate of up to 40  $Mhits/s$  with a maximum of 8  $Mhits/s$  on each strip. During the NA48/2 runs the KABES detectors had to withstand  $\sim 20$  MHz of charged hadrons concentrated in a few  $cm^2$  and to meet these requirements, a Micromegas mesh with a 50  $\mu m$  amplification gap was chosen.

The KABES efficiency was close to 100% even with a  $\sim 2$  MHz peak rate on the strips located at the centre of the beam spot.

The operating point (gas amplification and threshold) is adjusted to reduce signal overlaps on a single strip while high detection efficiency is maintained. A mean cluster size of 1.5 strips per track corresponding to  $ToT \sim 35$  ns is obtained with 325 V on the meshes and a 30 mV discrimination threshold.

The quality of the pattern recognition and track fitting in KABES, obtained after careful alignment and calibration, was studied using large samples of  $K^\pm \rightarrow \pi^\pm \pi^+ \pi^-$  decays reconstructed with the DCH spectrometer.

An important factor to ensure a good track association in KABES is the time resolution. The precise time of each track hit is obtained from the leading time and corrections derived from the  $ToT$  to account for slewing effects that can be as large as 15 ns.

The time resolution of KABES is obtained by comparing the track time measured in the beam spectrometer with the event time of the  $3\pi$  charged decay products recorded by the trigger hodoscope. The KABES track time resolution is found to be less than 0.6 ns, corresponding to a space resolution in the horizontal drift direction of  $70\ \mu\text{m}$ .

Moreover tests of a prototype, performed in November 2001, demonstrated a spark probability per track below  $10^{-9}$ .

## 8.4 KABES $25\ \mu\text{m}$ mesh

### 8.4.1 Improvement of rate capability

The overlap rate of signals on a micro-strip is proportional to their time duration, which is strongly correlated to the time over threshold ( $ToT$ ). Since the end of the signal occurs when the last ions created in the avalanche process reach the mesh, a smaller amplitude gap is expected to bring improvement in time occupancy. Figure 9 shows the  $ToT$  measurements of signals detected on strips located in front of identified tracks for detectors with amplification gap of  $25\ \mu\text{m}$  and  $50\ \mu\text{m}$ , respectively. The signal width is clearly reduced, with an improvement factor of about two. The FADC analysis of the data confirm a similar reduction on the overlapping rate. Extra improvements might be achieved with a still smaller gap, possibly down to  $10\ \mu\text{m}$ , with a different gas mixture and with faster front-end electronics.

### 8.4.2 High rate Behaviour

During the last day of data taking the rate was increased to a level approaching that needed for NA48/3. The behaviour of KABES was controlled by measuring the mesh current which senses the charge flow collected during the flat-top of the burst. This current is proportional to the number of tracks through the detector and to the amplification gain. No gain saturation was observed at the highest rates which means the devices still have good detection efficiency and therefore such detectors are good candidates for the proposed beam spectrometer.

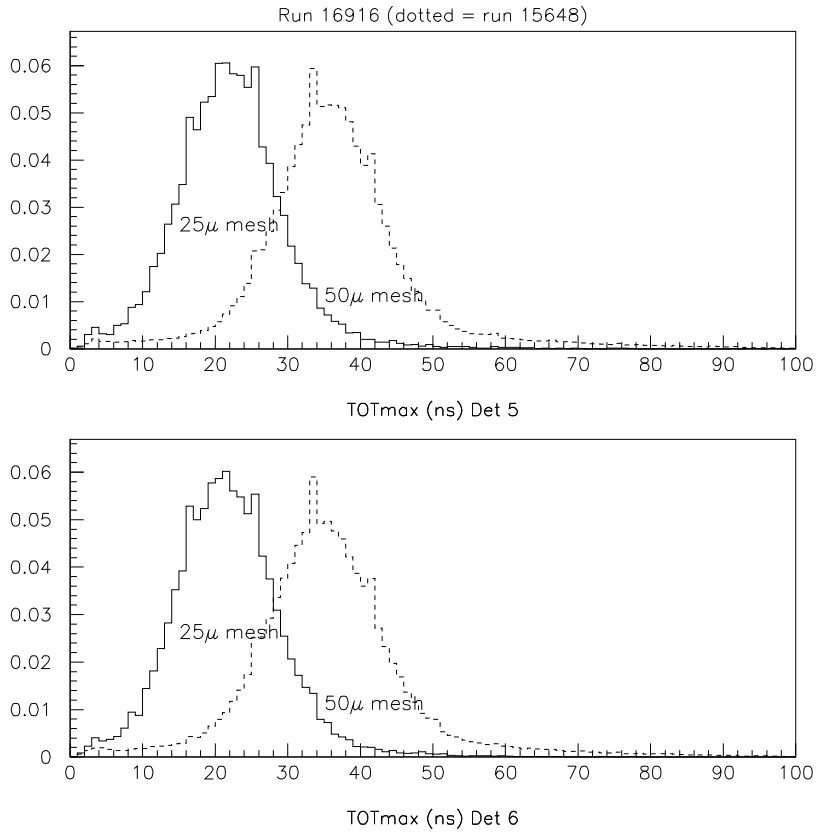


Figure 9: Comparison of 25 and 50  $\mu$  m KABES amplification gaps.

## 8.5 KABES FADC Read-out

### 8.5.1 FADC read-out test

A feasibility test of the KABES detector using a read-out based on 1 *GHz* FADC boards was performed in June and August 2004. It was possible to take data utilising, at the same time, the FADC read-out and the usual TDC one by replacing 18 amplification cards on 2 detectors with additional output for the FADC boards. By this way the KABES signals were digitized by specially developed 1 *GHz* FADCs.

Moreover a new KABES station was installed, different from that used during the NA48/2 data taking, with thinner Micromegas meshes of 25  $\mu\text{m}$ . A scan in beam intensity was performed from the nominal NA48/2 value up to 14 times the nominal intensity.

A Fast Analog-to-Digital Converter (FADC) was developed for the NA48 tagging system to digitize photomultiplier pulses and to recognize superimposed double pulses of protons crossing the tagging detector [28].

Each FADC module consists of two 8 bit FADC chips running at a sampling rate of 480 MHz. They can be interleaved to obtain one channel with an effective sampling rate of up to 960 Megasamples per second (960 MHz).

### 8.5.2 Results from the Test

A preliminary test of the prototype KABES station with a 25  $\mu\text{m}$  mesh was performed in June. The downstream KABES station was completely removed from the beam line and the new one was installed with splitters for strip signals to the FADC modules and TDCs. This time was precious to test both the new KABES detector and the FADC readout. Many different readout parameters were changed to match the desired configuration and to be able to cross-check the FADC data with the data from the TDC standard readout. The average value of the  $ToT$  obtained with the thinner mesh was of  $\sim 20$  ns, considerably lower than the  $\sim 35$  ns value obtained with the 50  $\mu\text{m}$  mesh.

A second test took place in August 2004, when the same 25  $\mu\text{m}$  mesh KABES prototype was installed in place of the downstream station and the upstream UP station was also equipped with signal splitters. The four central strips of the two complementary TPCs in the upstream UP station and the five plus five central strips of the last station were read out: thus making it possible to read out 18 KABES strips with the FADC modules. However only 9 FADC boards were available: therefore the strips were sampled at 480 MHz to be able to read-out 18 channels. For each trigger request a time window of  $\sim 600$  ns was read out in order

to be able to match the usual TDC read-out window. During normal data taking a digital zero-suppression was done to reduce the data volume: all data below an adjustable threshold are removed unless they are within 2 time-slices of an above-threshold sample. For detailed detector studies the zero-suppression mechanism was turned off to measure the electronic noise.

Figure 10 shows a typical event with not zero-suppressed data. This is a “scope picture” of a single KABES strip in a very high rate charged hadron beam (16 times the nominal NA48/2 beam intensity). One can clearly see four different pulses in the full 600 ns FADC readout time window, together with the baseline variation (the signal baseline is set to 20 ADC counts). From the information given in these plots it was also possible to determine the best value for the zero-suppression threshold.

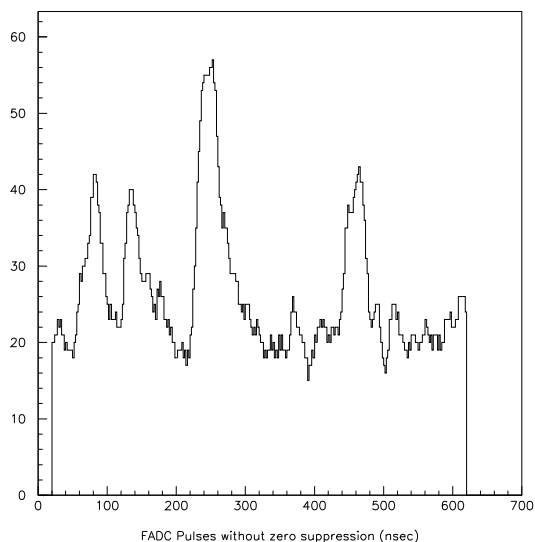


Figure 10: Multiple pulses in a KABES strip in case of not zero-suppressed FADC data.

Figure 11 shows a set of hits in a single KABES strip in the same beam configuration with zero-suppression enabled (the time scale in this plot and the following is  $2 \times 1.04$  ns, because of the 480 MHz sampling mode). It is clear that this level of discrimination between individual particles can be obtained only with the FADC read-out: the TDC could provide only the initial leading and final trailing time of the whole set of hits.

Unresolved double pulses may result in wrong timing and consequently in mistagging of kaon decays. Therefore the double pulse separating power is an important parameter for the performance of the FADC read-out.

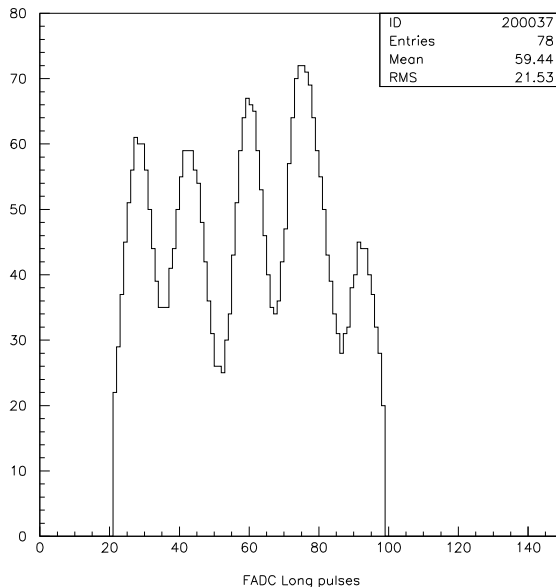


Figure 11: Multiple pulses in a KABES strip for zero-suppressed FADC data.

To determine the time of a particle passing the KABES detector, all the sampled strip pulses will be fitted during offline analysis. A first attempt to fit these pulses has been made and the following 4 parameter function has shown good results:

$$P_1 \times [1 + P_4 \times (t - P_2)] \times e^{-\frac{(t-P_2)^2}{2P_3^2}}$$

Figure 12 shows a sample of fitted pulses with different widths. Selecting pulses with a time duration less than a fixed value (assuming therefore that they are single and not overlapping) and assigning an uncertainty of 1.7 counts per FADC value it is possible to get a reduced  $\chi^2$  of 1 and to fit  $\sim 90\%$  of these "single pulses". The plot at the bottom right shows the reduced  $\chi^2$  distribution for a set of successful fits. The underflows are fit failures and the overflows are likely to be double pulses.

An example of the implementation of the fitting procedure to an event with multiple pulses is shown in Figure 13. Five peaks are clearly visible, while a sixth could be hidden on the right end part of the plot: a fit made assuming six peaks gives very good  $\chi^2$ .

### 8.5.3 Conclusions

KABES has been operated successfully in a high-intensity charged hadron beam. It provides accurate momentum, time and spatial coordinate measurements of charged particles.

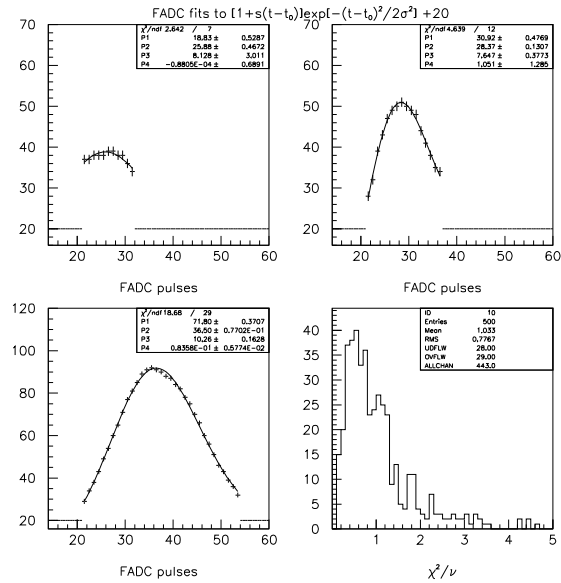


Figure 12: Fits of a small, medium and large pulses and the reduced  $\chi^2$  distribution for a set of successful fits

The tests performed with thinner Micromegas meshes of  $25 \mu\text{m}$  have given excellent results. They produce shorter pulses with a width of about 20 ns, thus allowing the detector occupancy to be significantly reduced.

It is clear from these very preliminary results that many improvements of the tagging capability of this beam spectrometer can be obtained by using a FADC read-out system. However, the main advantage of using a FADC read-out is to avoid pile-up due to the very high particle rate in the beam, thus providing a very efficient tracking system.

## 9 Time Schedule

- 2004
  - Launch GIGATRACKER R&D
  - Vacuum tests
  - Evaluate possible straw tracker for magnetic spectrometer
  - Start realistic cost estimation
  - Complete analysis of beam-test data

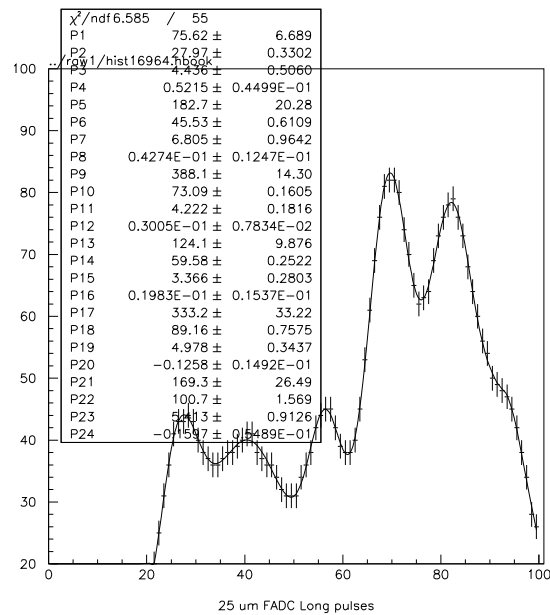


Figure 13: Fit of a "six pulse" event in case of very high particle rate (16 times the NA48/2 intensity).

- 2005
  - Continue all of the above
  - Complete specifications
  - Submit Proposal to SPSC
- 2006-2008
  - Construction, installation and tests of hardware including the new beam
- 2009-2010
  - Data Taking

## 10 Resources

The human, technical and financial resources needed to perform the experiment are being evaluated. In Table 12 we report a tentative indication of the cost of the detectors and associated electronics. The numbers are only intended to give an idea of the financial extent of the project.

Element	Cost (MCHF)	Comments
BEAM LINE	0.5	Modified K12 line
CEDAR	0.2	Replacement of Photon Detectors
GIGATRACKER	1.4	Assuming 0.13 $\mu\text{m}$ CMOS
VACUUM	0.7	Upgrade of the vacuum system
ANTI	4.2	Based on CKM estimate+ 40% for electronics
WC	3.0	Two more chambers
MNP33/2	2.5	Including prolongation of He tank
CHOD	1.0	Assuming 2 000 channels, 500 CHF/channel (PM r-o)
LKR	2.0	New supervision system + New Read-out and trigger (A state-of-the-art EM calorimeter would cost 15 MCHF)
MAMUD	2.0	Cost of the iron: 0.5 MCHF
SAC and CHV	0.5	
TRIGGER & DAQ	1.0	
TOTAL	19.0	

Table 12: Tentative indication of cost.

Human and technical resources are as important as the financial ones. We have started to identify the expertise needed to build the experiment. In particular we have identified the resources and we are ready to request the appropriate funding needed to launch the development of the GIGATRACKER, which is the most innovative element and is essential to the design based on the unseparated kaon beam.

## 11 Organization and Conclusions

This endeavour builds on the experience of the NA48 experiments. Last year a working group was launched to study possible rare kaon decay programme at the CERN-SPS. The results of the working group are reported in this document. We have found a fortunate combination where a compelling physics case can be addressed with an existing CERN accelerator, and employing a significant amount of infrastructure from an existing experiment. We stress that the new experiment is by no means a mere continuation of NA48 and that equipment investment of no less than 20 MCHF is needed to address the physics under study. Manpower, maintenance and operation, overheads and contingency may raise the total cost of

the project towards 30 MCHF over 5 to 6 years.

The NA48 working group has now evolved into a proto-collaboration to which most of the NA48/2 institutions intend to collaborate as can be seen from the list of signatories of this document. Some groups are already quite advanced in the process of requesting support from their Funding Agencies. The proto-collaboration is not closed and we are seeking the qualified participations of new collaborators.

It is clear that, as far as running this experiment is concerned, there are already two approved competitors for beam time (filling LHC and CNGS). The extent of the project implies that there cannot in addition be a fixed target heavy ion programme nor any other experiment in ECN3 competing for proton beam time at the data taking stage of this experiment. We understand that protons can be delivered for fixed target physics even when the LHC is being operated with ions.

## References

- [1] S. Adler *et al.* [E787 Collaboration], Phys. Rev. Lett. **88** (2002) 041803 [arXiv:hep-ex/0111091].
- [2] <http://www.phy.bnl.gov/e949/>
- [3] T. Komatsubara, T. Nakano and T. Nomura, "Letter of Intent for Study of the Rare Decay  $K^+ \rightarrow \pi^+ \nu \bar{\nu}$  with Stopped Kaon Beam at J-PARC", <http://www-ps.kek.jp/jhf-np/L01list/pdf/L04.pdf>
- [4] P.S. Cooper, Nucl. Phys. Proc. Suppl. **99B** (2001) 121; <http://www.fnal.gov/projects/ckm/Welcome.html>
- [5] M. Battaglia, A. J. Buras, P. Gambino and A. Stocchi (eds.) CERN report CERN-2003-002-corr [hep-ph/0304132].
- [6] W.J. Marciano and Z. Parsa, Phys. Rev. D **53** (1996) R1.
- [7] G. Buchalla and A. J. Buras, Nucl. Phys. B **398** (1993) 285; **400** (1993) 225; **412** (1994) 106 [hep-ph/9308272];
- [8] M. Misiak and J. Urban, Phys. Lett. B. **451** (1999) 161 [hep-ph/9901278].
- [9] L. Wolfenstein, Phys. Rev. Lett. **51** (1983) 1945.

- [10] G. Buchalla and A. J. Buras, Phys.Rev. D **54** (1996) 6782-6789.
- [11] G. D'Ambrosio and G. Isidori, Phys. Lett. B. **530** (2002) 108 [hep-ph/0112135].
- [12] L. Littenberg, Phys. Rev. D39 (1989) 3322.
- [13] H.W.Atherton, et al.: Precise Measurements of Particle Production by 400 GeV/it c Protons on Beryllium Targets, CERN Yellow Report: CERN 80-07 (1980).
- [14] G.Brianti, N.Doble: The SPS North Area High Intensity Facility: NAHIF, CERN/SPS/EA 77-2, CERN/SPSC/77-72, SPSC/T-18 (1977).
- [15] NA48/2 Collaboration, *Status Report on Experiment NA48/2*, CERN/SPSC-2003-033, SPSC-M-707, October 23, 2003.
- [16] C.Bovet, et al.: The CEDAR Counters for Particle Identification in the SPS Secondary Beams, CERN Yellow Report: CERN 82-13 (1982).
- [17] K.L.Brown, et al.: TRANSPORT, A Computer Program for designing Charged Particle Beam Transport Systems, CERN Yellow Report: CERN 80-04 (1980).
- [18] K.L.Brown and Ch.Iselin: DECAY TURTLE, A Computer Program for simulating Charged Particle Beam Transport Systems, CERN Yellow Report: CERN 74-2 (1974).
- [19] Ch.Iselin HALO, A Computer Program to calculate Muon Halo, CERN Yellow Report: CERN 74-17 (1974).
- [20] M.Benedikt, R.Garoby, Editors: Report of the High Intensity Proton Working Group, CERN-AB-2004-022 OP/RF (2004).
- [21] B. Peyaud, "KABES: a novel beam spectrometer for NA48", Draft paper of the 10<sup>th</sup> Vienna Conference on Instrumentation , Vienna (Austria), February 2004
- [22] T. Nakano and Y. Kuno: A Study on Photon Detection Efficiency Using Real  $K_{\pi 2}$  Data, E787 TN 256, 1993.
- [23] S. Ajimura, et. al., NIM A 435 (1999) 408.
- [24] K. Lang *et al.* [BNL E871 Collaboration], Nucl. Instrum. Meth. A 522 (2004) 274. [arXiv:physics/0308047].
- [25] A. Placci, Private communication.

- [26] Y. Giomataris *et al*, Nuc. Instrum. Methods A **376** (1996) 29-35.
- [27] Mota *et al*, “A Flexible Multi-Channel High Resolution Time to Digital Converter ASIC”, Nuclear Science Symposium, Lyon (France), October 2000
- [28] H. Bergauer *et al.*, Nucl. Instrum. Meth. A **419** (1998) 623-631